Interactions of Phenylalanine Derivatives with Human Tyrosinase: Lessons from Experimental and Theoretical tudies

Clarisse Faure, Yi Min Ng, Catherine Belle, Montserrat Soler-lopez, Lyna Khettabi, Mélissa Saïdi, Nathalie Berthet, Marc Maresca, Christian Philouze, Walid Rachidi, et al.

ChemBioChem

Research Article
doi.org/10.1002/cbic.202400235

Chemistry Europe
European Chemical Societies Publishing

www.chembiochem.org

Interactions of Phenylalanine Derivatives with Human Tyrosinase: Lessons from Experimental and Theoretical tudies

Clarisse Faure,[a] Yi Min Ng,[b] Catherine Belle,[a] Montserrat Soler-Lopez,[b] Lyna Khettabi,[b] Mélissa Saïdi,[b] Nathalie Berthet,[a] Marc Maresca,[c] Christian Philouze,[a] Walid Rachidi,[d] Marius Réglier,[c] Amaury du Moulinet d'Hardemare,*[a] and Hélène Jamet*[a]

The pigmentation of the skin, modulated by different actors in melanogenesis, is mainly due to the melanins (protective pigments). In humans, these pigments' precursors are synthetized by an enzyme known as tyrosinase (TyH). The regulation of the enzyme activity by specific modulators (inhibitors or activators) can offer a means to fight hypo- and hyper-pigmentations responsible for medical, psychological and societal handicaps. Herein, we report the investigation of phenylalanine derivatives as TyH modulators. Interacting with the binuclear copper active site of the enzyme, phenylalanine derivatives combine effects induced by combination with known resorcinol inhibitors and natural substrate/intermediate (amino acid part). Computational studies including docking, molecular dynamics and free energy calculations combined with biological activity assays on isolated TyH and in human melanoma MNT-1 cells, and X-ray crystallography analyses with the TyH analogue Tyrp1, provide conclusive evidence of the interactions of phenylalanine derivatives with human tyrosinase. In particular, our findings indicate that an analogue of *L*–DOPA, namely (*S*)-3-amino-tyrosine, stands out as an amino phenol derivative with inhibitory properties against TyH.

1. Introduction

Tyrosinase (Ty, EC 1.14.18.1) is an ubiquitous enzyme, belonging to type-3 copper enzyme, present in fungi,[1–3] bacteria,[4–6] insects,[7] plants[8,9] and mammals. To date, only one X-ray crystal structure of an associated tyrosinase enzyme (Tyrosinase-related protein 1, Tyrp1) has been reported for a human tyrosinase.[10] Tyrp1 contains a dinuclear zinc site (in place of the expected dicopper site)[11] although it displays the typical tyrosinase folding. The active site is highly conserved in all tyrosinases (Tys), and is composed of two copper atoms coordinated by three nitrogen atoms from neighbouring histidine residues. Three identified dicopper active site states are observed through the catalytic cycle: *deoxy* (Cu^{I}…Cu^{I}), *met* (Cu^{II}-(OH)-Cu^{II}) and *oxy* (Cu^{II}-O_2^{2-}-Cu^{II}) forms.[12,13] The later exhibits molecular dioxygen in a side-on (μ-η^2:η^2) bridging mode (Scheme 1A). Using molecular dioxygen, tyrosinases catalyze hydroxylation of monophenols to respective o-quinones by a four-electron process (phenolase activity) as well as oxidation of *o*-diphenol substrates to *o*-quinone (catecholase or diphenolase activity).[14,15] In all organisms, Tys are involved in the biosynthesis of protective pigments.[16] In humans, tyrosinase (TyH) is the first enzyme of the multistep process of melanogenesis. It catalyzes the hydroxylation of *L*-tyrosine to *L*-dihydroxyphenylalanine and the following oxidation of *o*-diphenol to the corresponding quinone, *L*-dopaquinone (Scheme 1B), which is the key intermediate in melanin (photo protective pigment) biosynthesis. Melanin-related disorders are known to cause hyperpigmentation[17] and severe skin lesions.[18,19] As Ty inhibition is a well-established approach for controlling melanin production, development of Ty inhibitors has raised a considerable interest in cosmetic and pharmaceutical industries.[20]

Despite the large number of Ty inhibitors described in the literature based on in vitro assays, only few have proven relevant in clinical trials[21] or in industrial applications[13,22] since most of the studies have been performed almost exclusively using mushroom or bacterial Ty enzymes. Furthermore, it is now demonstrated that the environment in the second coordination sphere residue among Tys from different organisms are different,[22–24] and consequently, extrapolation of the inhibition activity from one source to the others is hazardous. The low level of sequence homology among Tys and differences in the binding pocket topologies reported by different authors

[a] *Dr. C. Faure, Dr. C. Belle, Dr. N. Berthet, Dr. C. Philouze, Dr. A. du Moulinet d'Hardemare, Dr. H. Jamet*
Université Grenoble Alpes, CNRS
Department of Molecular Chemistry (DCM, UMR 5250), 38058 Grenoble Cedex 9 (France)
E-mail: helene.jamet@univ-grenoble-alpes.fr
Amaury.D-Hardemare@univ-grenoble-alpes.fr

[b] *Y. Min Ng, Dr. M. Soler-Lopez, L. Khettabi, M. Saïdi*
Structural Biology Group, European Synchrotron Radiation Facility (ESRF) 38053, Grenoble (France)

[c] *Dr. M. Maresca, Dr. M. Réglier*
Aix Marseille Université, CNRS, Centrale Marseille, iSm2, Marseille (France).

[d] *Prof. W. Rachidi*
IRIG-BGE U1038, INSERM, Univ. Grenoble Alpes, Biomics, 38054 Grenoble (France)

Supporting information for this article is available on the WWW under https://doi.org/10.1002/cbic.202400235

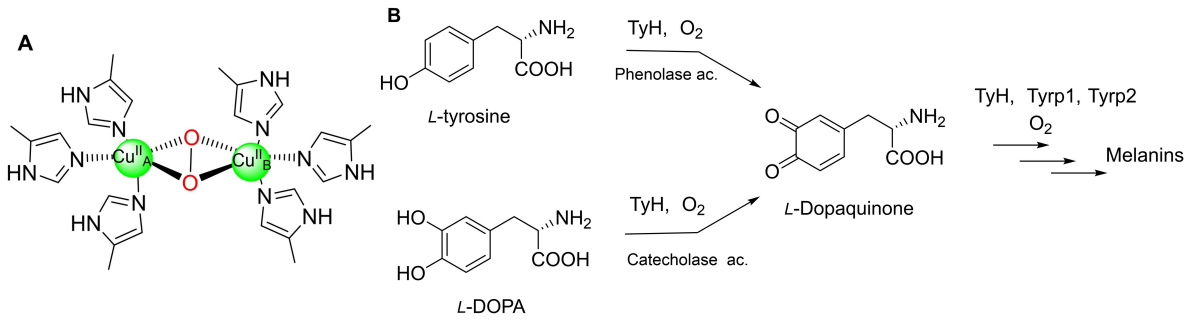

Scheme 1. A: Active site of Ty with oxygen atoms bound as a peroxide (Per) in a μ-η²:η² mode (*oxy*-form) and **B**: biosynthesis of melanins by human tyrosinase and its related enzymes Tyrp1 and Tyrp2.

and comparative studies, has prompted us to find specific TyH inhibitors. To discover efficient TyH modulators, our strategy is based on the study of stabilized molecules with a structure close to the natural substrates (*L*-tyrosine and *L*–DOPA). These modulators are thus expected to mimic the natural molecules and able to establish interactions with the second shell of the active site via the side chain of *L*-tyrosine. Tyrosine analogs such as mimosine, kojic acid or tropolone are stabilized with the active site along aromatic stacking interactions with amino acid residues and additional hydrogen bondings.[10] Besides, tyrosinase inactivation by resorcinol based-compounds[25] have been previously reported on mushroom, potato and bacterial tyrosinases with the recognized 2,4-substituted resorcinol moiety embedded in various scaffolds.[23,26,27,28,29] In humans, the resorcinol motifs like the 4-butylresorcinol,[30] the thiamidol (isobutylamido-thiazolyl-resorcinol)[22] (Figure 1A) or others modified derivatives[31,32] have been also reported as inhibitors of TyH and/or melanins. However, the full potential of resorcinol derivatives on TyH needs to be further explored.

In this study, as the hydroxyl group's positioning has been shown to be an important parameter for activity, we have examined the racemic 2,4-dihydroxyphenylalanine and for comparison purposes, the racemic 3,5-dihydroxyphenylalanine. The phenylalanine derivatives represent a combination of resorcinol and amino acid moieties (similar to *L*-tyrosine, the natural substrate or *L*–DOPA intermediate) and for which we hypothesize a better target for the TyH active site, leading to more selective and potent inhibitors. Additionally, amino phenols, recognised as mushroom tyrosinase substrates[33–35] capable to bind to the dicopper center, are of interest to understand the influence of the phenol position on the modulation of the activity of the enzyme. Furthermore, we have investigated an analogue of *L*–DOPA, the *(S)*-3-amino-tyrosine, an amino phenol that shares the same stereochemistry as the DOPA molecule (Figure 1B).

The first step of our investigation involved modelling studies using a human tyrosinase model. Following molecule synthesis, we carried out biological activity assays on TyH and a structural analysis with Tyrp1 by X-ray crystallography. The results were consistent with the computational studies, including molecular dynamics and free energy calculations on the model of TyH, and provide further insights into the interaction modes of these phenylalanine derivatives with the tyrosinase active site.

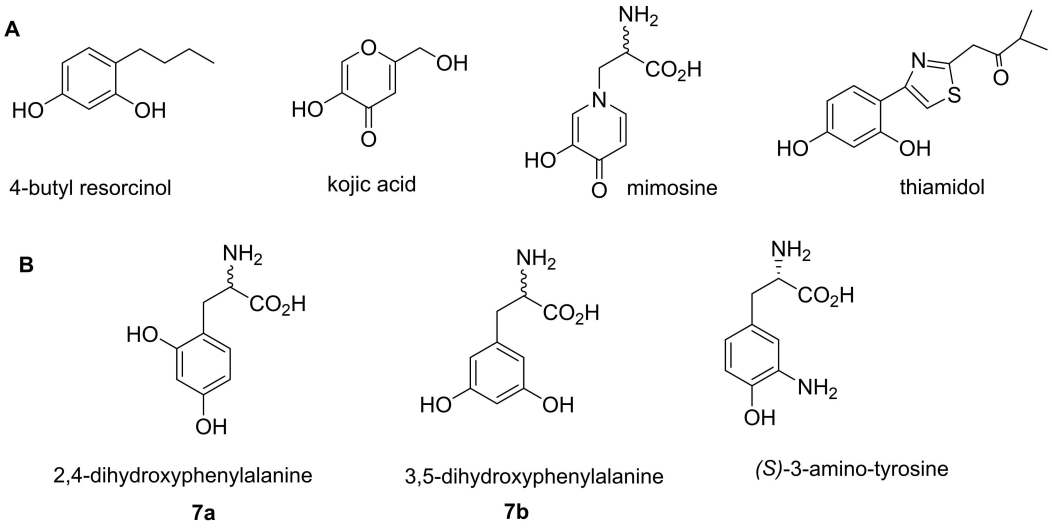

Figure 1. A: Structure of reference tyrosinase inhibitors, **B**: Structure of molecules studied in this work.

2. Results and Discussion

2.1. Docking Study

The docking study was done using a homology model of TyH based on the crystallographic structure of Tyrp1 (PDB: 5 M8P),[10] reported in a previous publication[36] and exhibiting a high degree of similarity to the model predicted by the AlphaFold approach[37] (AF–P14679-F1 model_v2). As described in the methods, we employed the software Autodock.[38] We investigated the binding interactions of the three molecules – *rac*-2,4 phenylalanine, *rac*-3,5 phenylalanine and (*S*)-3-amino-tyrosine - (Figure 1B) and compared them with that of the natural substrate *L*–DOPA. Molecules were docked on the *oxy* form of TyH in their enantiopure form *(S)*, with the same stereochemistry as the *L*–DOPA. We selected the *oxy* form since it is the active form in the mono and diphenolase enzymatic processes and the three selected molecules are expected have both activities (Figure 1B). With the docking procedure, 100 positions were generated, and the one that occurred most frequently with the lowest scoring function, was chosen as the suitable binding mode. These positions are illustrated in Figure 2 with a representation of the main interactions.

All the molecules appear to effectively bind to the active site, resembling the binding pattern of *L*–DOPA. This is characterised by a strong hydrogen-bond network, in particular between one of their oxidizable groups and the peroxo group (Per) of the *oxy* form, along with a serine residue (Ser380). The distances between the hydrogen of the oxidizable moiety and one oxygen of the Per group are 2.0, 2.1, and 2.1 Å, respectively, for *(S)*-3,5-dihydroxyphenylalanine, *(S)*-2,4 dihydroxyphenylalanine and *(S)*-3-amino-tyrosine. In all three molecules, hydrogen-bonding interactions occur between Asn364 and the functional groups on the aromatic cycle, as well as between Ser375 and the NH_3^+ group of the studied molecule. Moreover, their CO_2^- group interacts with the Ser360 and the Lys306 residues. As the three molecules adopt a close position to *L*–DOPA, the two resorcinol's molecules in their racemic form were synthetized and separated later depending whether biological or co-crystallization assays were conclusive. The *(S)*-3-amino-tyrosine is commercially available.

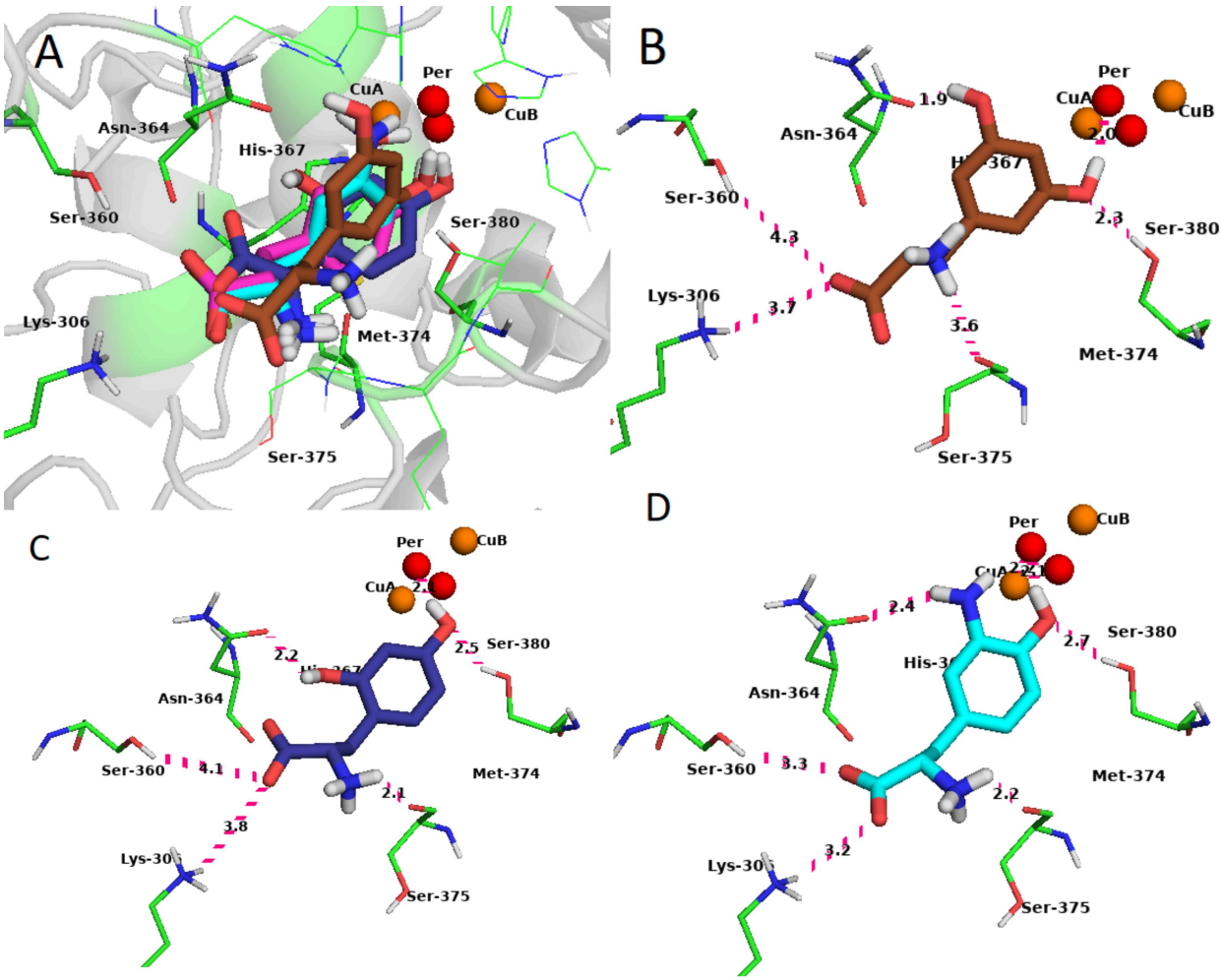

Figure 2. A. Superposition of the docking position of the three *(S)*-enantiomers along with the *L*–DOPA docking position (in magenta). Per designs the peroxo group presents in the *oxy* form of TyH. *(S)*-3-amino-tyrosine in turquoise. *(S)*-3,5-dihydroxyphenylalanine in brown. *(S)*-2,4-dihydroxyphenylalanine in blue. Plots of the main interactions with: **B**. *(S)*-3.5-dihydroxyphenylalanine, **C**. *(S)*- 2,4-dihydroxyphenylalanine and **D**. *(S)*-3-amino-tyrosine.

2.2. Racemic Compounds Synthesis

The racemic compounds were efficiently synthetized in 7 steps starting from the corresponding dihydroxybenzaldehydes (Scheme 2) by variations of published procedures.[28,29] We were inspired by Lambooy's work for the synthesis of these isomers following the classical Erlenmeyer-Plöchl amino acid method which introduces the azlactone precursor motif of the amino acid as a key step.

The phenols of the 3,5- and 2,4-dihydroxybenzaldehyde (Scheme 2) were first protected to avoid competing with coumarin formation (which would be the case with unprotected 2,4-dihydroxybenzaldehyde) in step 2 of azlactone formation,[39] and to simplify the otherwise tedious purifications. Under these conditions, the condensation of aldehydes (**1 a, b**) with hippuric acid led to azlactones (**2 a, b**) in satisfactory yields. The preliminary opening of the azlactone by methanolysis in step 3, facilitated the catalytic hydrogenation at room temperature of the benzylidene moiety (**4 a, b**; quantitative yield). The next steps consisted of the successive deprotection of the phenols (**5 a**, **b**), the acid (**6 a, b**) and finally the amine (**7 a, b**). Purification was done by HPLC in order to obtain compounds with an optimal purity degree.

2.3. Biological Activity Assays using Isolated TyH and Melanoma Cells

To study the efficiency of phenylalanine derivatives as TyH modulators, we produced recombinant human tyrosinase in insect cells as previously described.[40] Determination of Michaelis-Menten kinetic parameters (K_M and V_M) for *L*–DOPA oxidation by plotting the initial rate of DOPAchrome formation (v_i) versus the concentration of *L*–DOPA was performed. From the corresponding curves, $K_M = 2.2 \pm 0.5$ mM and $V_M = 0.0020 \pm 0.0002$ mM.s^{-1} were determined (Figure S1). These values differ from the previous ones reported in the literature ($K_M \approx 0.3$-0.8 mM).[22,41,42] However, this disparity could be attributed to the TyH fragment employed (full-length protein vs. intramelanosal segment and absence of the membrane region).

The efficiency of the phenylalanine derivatives as TyH modulators was first evaluated through a competitive assay. For that, the diphenolase activity of the isolated TyH, *i.e* the oxidation of *L*–DOPA to DOPAchrome, was investigated in presence of various concentrations of each compound, with absorbance measured at 475 nm. The IC_{50} values determined for all phenylalanine derivatives are reported in Table 1.

For both resorcinol derivatives *rac*-(**7 a**) and *rac*-(**7 b**), no inhibition or activation of the diphenolase activity was observed (Table 1). In contrast, *(S)*-3-amino-tyrosine resulted in an inhibitory activity with an IC_{50} of 0.07 ± 0.01 mM (Figure S2A).

Comparison of the IC_{50} values with those reported in the literature is challenging due to their dependency on the experimental conditions. Thus, biological assays were per-

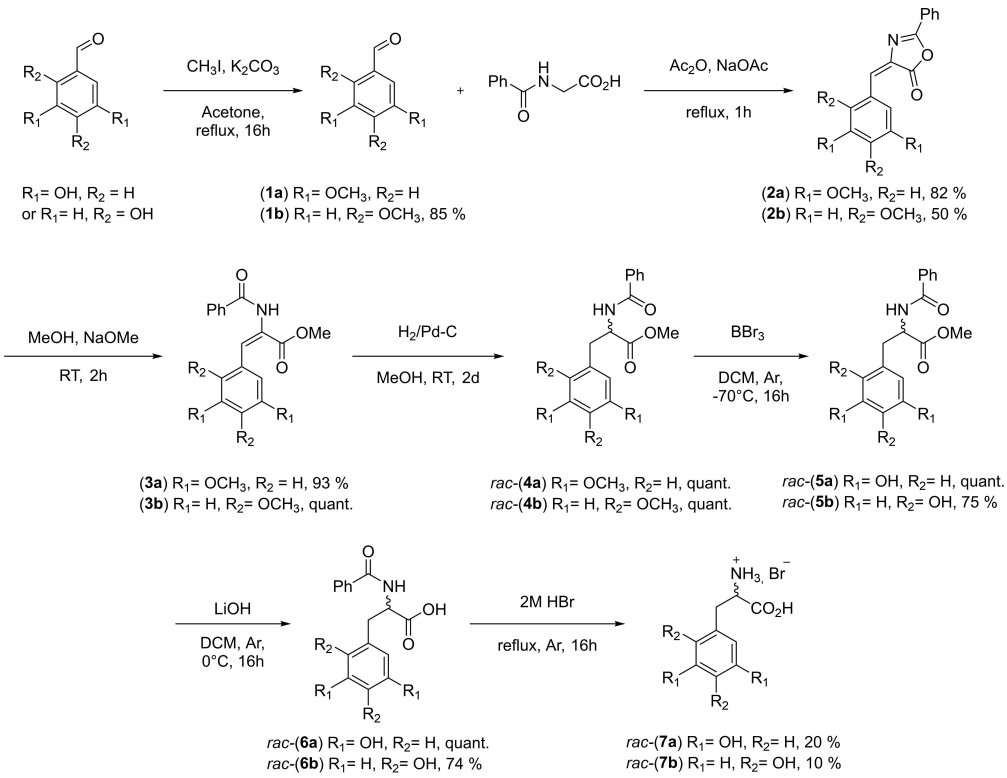

Scheme 2. Synthesis of *rac*-3,5- and *rac*-2,4-dihydroxyphenylalanines respectively *rac*-(**7 a**) and *rac*-(**7 b**).

Table 1. IC_{50} determined for phenylalanine derivatives relative to the diphenolase activity of TyH.

Molecules	IC_{50} (mM)
(S)-3-amino-tyrosine	0.07 ± 0.01
rac-(**7 a**)	> 1 [a]
rac-(**7 b**)	> 1 [a]

[a]: No activity observed in the concentration of study. Conditions: 2.4 mM de L–DOPA, 0.012 mg/ml of TyHs, PBS buffer at pH 7.0, concentration of the phenylalanine derivatives: 0.04 – 1 mM

formed on (*S*)-3-amino-tyrosine to determine the inhibition constant (K_I). By examining varying concentrations of *(S)*-3-amino-tyrosine, initial rates were established at various *L*–DOPA concentrations. From Lineweaver-Burk plots of the initial velocity (v_i) for increasing concentrations of *L*–DOPA in presence of different concentrations of *(S)*-3-amino-tyrosine (Figure S2B), the observed inhibition behaviour for the aminophenol compound on isolated TyH was typical of mixed inhibitors, as indicated by previous studies.[41,43] Sets of $1/V_M^{APP}$ and of K_M^{APP}/V_M^{APP} were used for the determination of the inhibition constants K_I (Eq. 1 and 2):

$$\frac{1}{V_M^{APP}} = \frac{1}{V_M}\left(1 + \frac{[I]}{K_{IU}}\right) \quad (1)$$

$$\frac{K_M^{APP}}{V_M^{APP}} = \frac{K_M}{V_M}\left(1 + \frac{[I]}{K_{IC}}\right) \quad (2)$$

where, [*I*] is the inhibitor concentration, K_{IU} is the uncompetitive constant of inhibition and K_{IC} the competitive one. The inhibition constants K_{IU} and K_{IC} were determined from Eq. 1 and 2, respectively. According to Eq. 1, the linear regression of the $1/V_M^{APP}$ *vs.* [*I*] plot leads to the K_{IU} constant. The same treatment according to Eq 2, the K_M^{APP}/V_M^{APP} *vs.* [*I*] plot leads to the K_{IC} constant (Figure S2C) and we find $K_{IC} = 0.10 \pm 0.02$ mM and $K_{IU} = 0.09 \pm 0.08$ mM.

We then evaluated the inhibition potential of *(S)*-3-amino-tyrosine in both cell lysates and intact cells using human melanoma MNT-1 cells. TyH inhibition in cell lysates yielded an IC_{50} of 0.08 ± 0.01 mM (Figure S3A), confirming the ability of *(S)*-3-amino-tyrosine to prevent melanogenesis within the intricate cytoplasmic milieu of human cells. The proximity of this value to the one obtained with isolated TyH (Figure S2A) indicates the specific activity of this compound on TyH. The evaluation of its tyrosinase activity on whole MNT-1 cells (Figure S3B) revealed around 50% of activity inhibition at 1 mM of *(S)*-3-amino-tyrosine, demonstrating its ability to cross the MNT-1 cell membrane without concomitant cytotoxicity ($DL_{50} \geq 6$ mM, Figure S3C).

Altogether, these results position the (*S*)-3-amino-tyrosine as the preferred candidate to effectively inhibit the processes of melanogenesis in a cell-based environment.

X-Ray crystallographic analysis of Tyrp1 in complex with *(S)*-3-amino-*L*-tyrosine and the racemic 2,4- and 3,5 dihydroxyphenylalanine molecules

Since crystallization of TyH remains a challenge, X-ray crystallographic analysis is done on Tyrp1. As mentioned above, Tyrp1 shares 70% sequence similarity with TyrH and also exhibits effective interaction with recognised TyrH substrates.[10] Notably, given that the Tyrp1 active site resembles that of TyH despite containing zinc (Zn) instead of copper (Cu), we anticipate that no oxidation reaction should occur, allowing the analysis of the specific position of the molecule in the active site. If a compound binds the active site, this is a strong indication that it may be a substrate or, at the very least, have a high affinity for that particular site. Therefore, we carried out the structure determination of Tyrp1 in complex with (*S*)-3-amino-tyrosine and the racemic compounds **(7 a)** and **(7 b)**, respectively, to examine how these molecules bind within the tyrosinase active site.

Crystals of native intramelanosomal Tyrp1 diffracted at 2.35 Å in the ESRF beamline ID23-2,[44] with one molecule per asymmetric unit in space group $P322_1$ (Table 2, TYRP1). The crystal structure reveals a compact globular shape, with tight interactions between the Cysteine-rich and tyrosinase subdomains, similar to the previously reported structure (Figure 3).[10] As previously reported[10], we confirmed that the active pocket of Tyrp1 consists of two Zn ions coordinated by six histidine residues and a bridging water molecule, which closely resembles the type-3 binuclear copper centre of Tys. With 3.5 Å distance between the two Zn atoms, Zn–A is directly coordinated by His192, His215 and His224, while Zn–B is directly coordinated by His377, His381 and His404.

Subsequently, in order to characterize the binding mode of the selected compounds with Tyrp1, various X-ray crystallographic methods were attempted. Soaking of compounds were

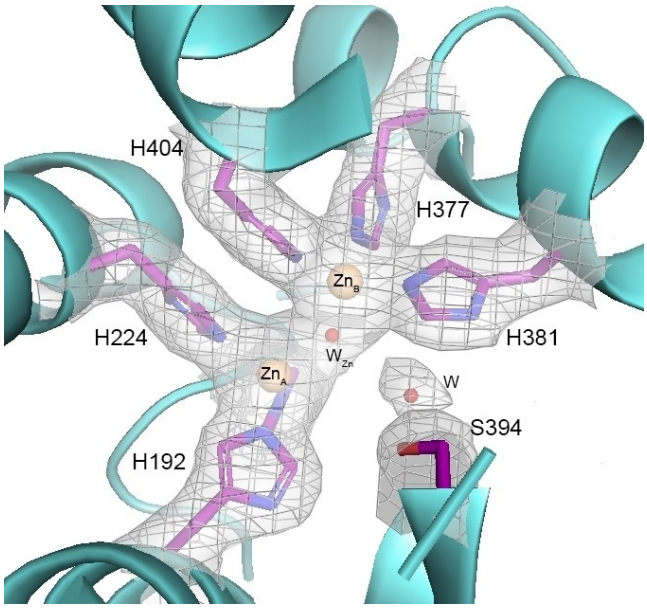

Figure 3. Close-up of the Tyrp1 active site shown with the *2Fo – Fc* electron density map (gray wire) contoured at 1 σ level. Zn ions are shown as orange spheres with the bridging water molecule in red (W_{Zn}). Numbering of Histidine residues is indicated.

Table 2. X-ray crystallography data collection, refinement, and validation statistics. TYRP1 is the X-ray crystal structure of apo (native) Tyrp1, TYRP1-ALT(*S*) refers to Tyrp1 in complex with *(S)*-3-amino-*L*-tyrosine, and TYRP1-24*S* and TYRP1-24*R* refer to Tyrp1 in complex with the racemic 2,4 dihydroxyphenylalanine molecule refined respectively with the (*S*) and (*R*) enantiomers.

	TYRP1 apo	TYRP1-24R	TYRP1-24S	TYRP1-ALT(S)
PDB id	9EY6	9EY7	9EY5	9EY8
Beamline	ID23-2	ID30B	ID30B	ID30 A1(MASSIF-1)
Wavelength (Å)	0.8731	0.8856	0.8856	0.9655
Resolution range (Å)	34.83 –2.236 (2.29–2.24)	48.33 –2.607 (2.7 –2.61)	48.33 –2.607 (2.7–2.61)	47.26–2.198 (2.22 –2.2)
Space group	*P* 3_2 2 1	*P* 3_2 2 1	*P* 3_2 2 1	*P* 2_1 2_1 2_1
Unit cell dimensions a, b, c (Å) α, β, γ (°)	103.754, 103.754, 140.988 90, 90, 120	103.152 103.152 138.509 90 90 120	103.152, 103.152, 138.509 90, 90, 120	88.972, 126.973, 212.339 90, 90, 90
Total reflections	357813 (15676)	155516 (15693)	155516 (15693)	805840 (19674)
Unique reflections	81266 (3810)	47641 (4767)	47641 (4767)	234158 (6894)
Multiplicity	4.4 (4.1)	3.3 (3.3)	3.3 (3.3)	3.4 (2.9)
Completeness (%)	99.06 (86.53)	98.63 (98.33)	98.63 (98.33)	99.51 (88.35)
Mean I/sigma(I)	6.55 (0.75)	4.94 (1.01)	4.94 (1.01)	8.29 (0.59)
Wilson B-factor	44.72	56.46	56.46	40.36
R-merge	0.1136 (1.158)	0.1412 (0.6955)	0.1412 (0.6955)	0.0886 (1.377)
R-meas	0.1295 (1.319)	0.164 (0.8078)	0.164 (0.8078)	0.1052 (1.668)
R-pim	0.06149 (0.6229)	0.08136 (0.4014)	0.08136 (0.4014)	0.05616 (0.9268)
$CC_{1/2}$	0.994 (0.46)	0.988 (0.598)	0.988 (0.598)	0.996 (0.395)
CC*	0.999 (0.794)	0.997 (0.865)	0.997 (0.865)	0.999 (0.752)
Reflections used in refinement	42627 (2448)	26211 (2593)	26211 (2593)	122304 (3633)
Reflections used for R-free	2105 (100)	1356 (133)	1356 (133)	6087 (178)
R-work	0.1754 (0.2939)	0.1958 (0.2995)	0.1953 (0.3004)	0.1889 (0.4127)
R-free	0.2152 (0.3211)	0.2371 (0.3113)	0.2352 (0.3081)	0.2324 (0.4704)
Number of non-hydrogen atoms	4050	3845	3845	16585
macromolecules	3602	3571	3571	14334
ligands	279	216	216	1252
solvent	169	58	58	999
Protein residues	447	447	447	1791
RMS (bonds)	0.011	0.009	0.008	0.008
RMS (angles)	1.66	1.07	1.06	1.03
Ramachandran favored (%)	95.73	94.16	94.16	95.46
Ramachandran allowed (%)	4.27	5.84	5.84	4.49
Ramachandran outliers (%)	0.00	0.00	0.00	0.06
Rotamer outliers (%)	4.00	2.53	2.53	1.32
Clashscore	9.98	5.34	5.06	3.76
Average B-factor	56.33	61.73	61.86	43.57
macromolecules	53.11	60.67	60.80	41.01
ligands	101.18	80.45	80.76	72.59
solvent	50.89	57.06	56.84	44.30

initially trialled with well-diffracting Tyrp1 crystals before co-crystallization approach was utilized.

2.3.1. Racemic 2,4-Dihydroxyphenylalanine

Tyrp1 crystals soaked with racemic 2,4-dihydrophenylalanine at 9 mM concentration were subjected to X-ray diffraction data collection in the ESRF beamlines MASSIF-3 (ID30 A-3)[45] and ID30B[46] followed by structure determination. At 2.6 Å resolution, we observed electron density occupying the active pocket

of Tyrp1, corresponding to the compound. Due to the racemic nature of compound used, models of both enantiomers were evaluated during structure determination (Table 2). Both enantiomers could be placed in the active pocket with the 4′-OH group making hydrogen bonding interaction with the bridging water at 2.8 Å distance (Figure 4). Apart from that, additional hydrogen bonding interactions were also observed between the 4′-OH group and the side chain of Ser394, the 2′-OH group and the side chain of Gly389, and the carboxyl group and the side chain of Arg374. All these hydrogen bonding interactions further strengthened the binding of 2,4-dihydrophenylalanine to Tyrp1's active pocket.

Using X-ray fluorescence, we confirmed the presence of zinc ions in the Tyrp1 active site, which was further corroborated by X-ray anomalous dispersion data collected at the zinc absorption edge (9.65 keV), which showed that the Tyrp1 zinc ions occupy the position of the copper ions in tyrosinase (Figure 4B).

2.3.2. 3,5-Dihydroxyphenylalanine

As for compound 3,5-dihydroxyphenylalanine, several soaking attempts with Tyrp1 crystals were tested in similar manner as for compound 2,4-dihydroxyphenylalanine. X-ray diffraction data collection in the ESRF beamlines MASSIF-3 (ID30 A-3)[45] and ID30B[46] and structure determination of soaked Tyrp1 crystals revealed no binding of the compound despite the high diffraction of the crystals at 2.2 Å resolution (Table 2). This result aligns with the lack of activity observed in the biological assays.

2.3.3. (S)-3-Amino-Tyrosine

For compound (*S*)-3-amino-tyrosine, several soaking attempts with Tyrp1 crystals were initially performed. Unfortunately, all soaking attempts resulted in non-diffracting crystals during data collection. However, co-crystallization trials of Tyrp1 with the compound resulted in a single crystal of approximately 80 μm in length that appeared after 33 days in a crystallization condition different from the native Tyrp1 crystals. X-ray diffraction data collection in the ESRF beamline MASSIF-1 (ID30 A-1)[47] led to a 2.2 Å resolution structure, revealing that Tyrp1 proteins were differently packed in this crystal system, with four molecules of Tyrp1 per asymmetric unit in space group $P2_12_12_1$ (Table 2). Electron density corresponding to (*S*)-3-amino-tyrosine was observed in one of the four Tyrp1 molecules (chain E) (Figure 5). With similar binding pose, (*S*)-3-amino-tyrosine makes hydrogen bonding interaction with the bridging water at 2.7 Å distance using its 3′-OH group. Additional hydrogen bonding interactions are also observed between the 3′-OH group and the side chain of Ser394 and another water molecule, as well as between the carboxyl group and the side chains of Tyr362 and Arg374. Additionally, the more compact packing of the $P2_12_12_1$ crystal system also provides additional support for the binding of (*S*)-3-amino-tyrosine in the active pocket, as observed by the hydrogen bonding interactions of the carboxyl group with the side chains of Arg471 and Asn473 at points making crystal contacts.

In summary, our crystallographic findings reveal that racemic 2,4-dihydroxyphenylalanine (**7 a**) (Figure 4) and (*S*)-3-amino-tyrosine (Figure 5) exhibit a strong affinity for the Trp1 active site, adopting a binding conformation similar to reference compounds reported earlier (kojic acid, mimosine, tropolone and tyrosine).[10]

2.4. Molecular Dynamics (MD)

Based on the X-ray studies and the biological assays, MD simulations were performed, taking the docking position of each molecule on the *oxy* form of a homology model of TyH as starting point (Figure 2 and Figure S4). Since the racemic

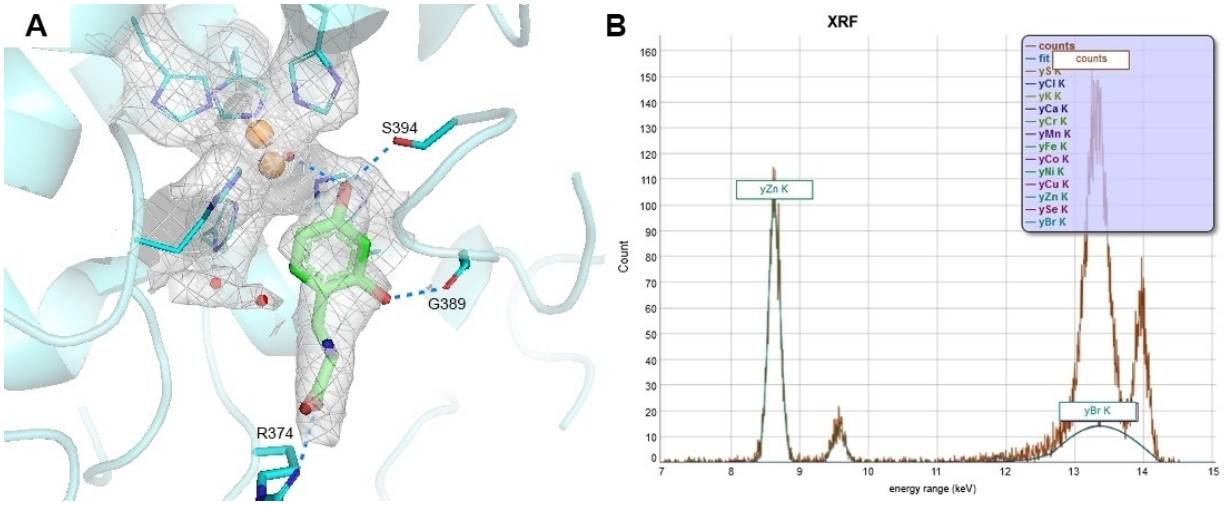

Figure 4. Crystal structure of the 2,4-dihydroxyphenylalanine bound to Tyrp1. (**A**) The 2 Fo- Fc electron density shows the *R* enantiomer binding mode, with the interacting residues highlighted. (**B**) X-ray fluorescence scan (XRF) of 2,4-dihydroxyphenylalanine-Tyrp1 crystals showing two peaks on the Zn K-alpha and K-beta absorption edges (8.6 and 9.65 keV respectively), confirming the presence of the ion. The two large peaks on the right of the spectrum are the Compton (inelastic) and the Rayleigh (elastic) scattering peaks of the incident beam.

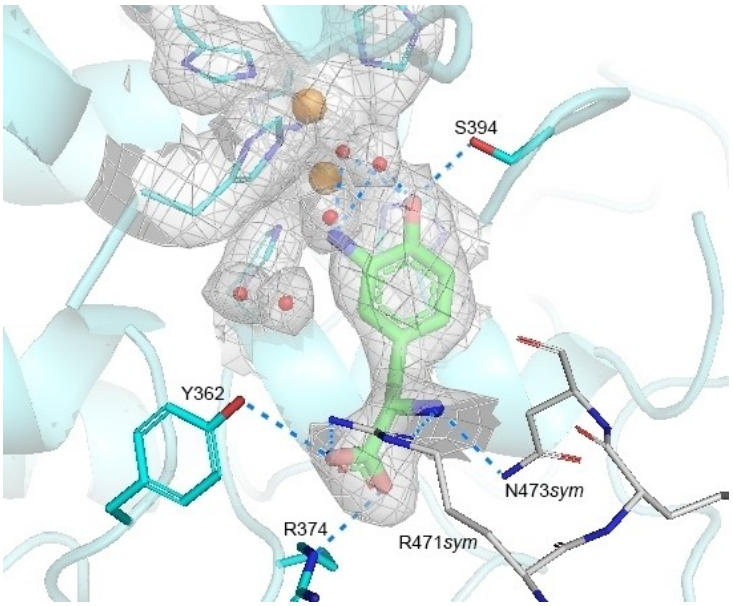

Figure 5. Crystal structure of the (*S*)-3-amino-tyrosine bound to Tyrp1. The 2 Fo–Fc electron density shows the observed binding mode, with the interacting residues and water molecules highlighted. Interestingly, the compound makes crystal contacts with a symmetry-related Tyrp1 molecule (in grey).

compounds (**7 a**) and (**7 b**) displayed different activity in the biological assays, each enantiomer was studied separately. Since all the molecules are placed in the active pocket without direct interaction with copper atoms, molecular dynamics can be used to compare their binding mode. Inclusion of a quantum part within QM/MM calculations is not mandatory and long simulation times can be considered. The MD was performed over a total duration of 100 ns for the two enantiomers of the 2,4- and 3,5-dihydroxyphenylalanine ((**7 a**) and (**7 b**)) and for the *(S)*-3-amino-tyrosine. To characterize the binding mode of the studied compounds in the active site, the distance (d_1) between an oxidizable atom of the molecule of interest and an oxygen atom of the Per group of the active site was followed as function of the time (Figure 6) and in parallel plots of the rmsd analysis on the protein are given in supporting information (Figure S5), confirming the validity of our MD simulations.

Based on the difference in interactions observed between the different oxidizable groups, *(S)*-3-amino-tyrosine appears to be the best candidate. The aminophenol motif remains fairly close to the active site with a distance d_1 around 2.5 Å up to 50 ns of simulation then around 3.5–4 Å up to 100 ns. This MD

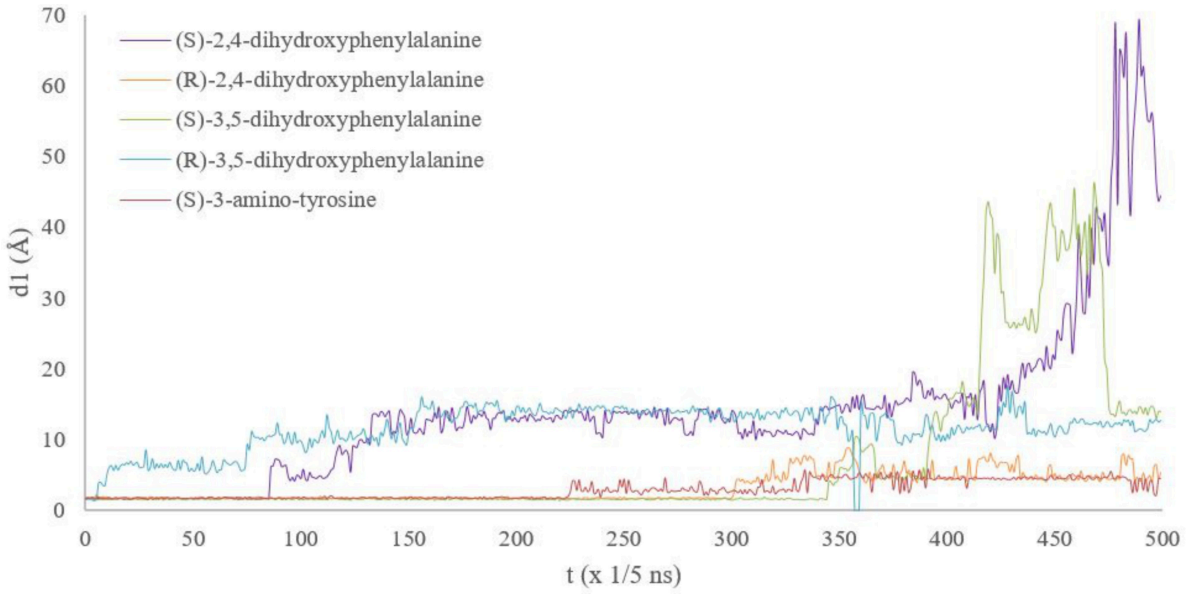

Figure 6. Evolution of the distance d_1 between an oxidizable atom of the phenylalanine derivatives and an oxygen atom of the Per group of the *oxy* form of a homology model of TyH as a function of the time (ns).

simulation was performed in triplicate and for the three simulations during all the 100 ns, molecule remains close to the active site with a distance under 4 Å (Figure S6). According to the criterion on d_1 in Figure 6, the second best candidate is the *(R)*-2,4-dihydroxyphenylalanine enantiomer, with a very stable distance of 2.25 Å up to 60 ns of simulation then an oscillation around 5.25 - 7.25 Å. In third position is the *(S)*-3,5-dihydroxyphenylalanine enantiomer, with a very stable d_1 of 2.25 Å up to 60 ns of simulation before to leave completely the active site with a d_1 increasing up to 40 Å. And finally, the *(R)*-3,5-dihydroxyphenylananine and *(S)*-2,4-dihydroxyphenylalanine molecules completely leave the active site with a distance d_1 changing from 2.0 Å to 6.0 Å in just 10 ns of simulation then from 6.0 Å to 14.0 Å or to 60 Å respectively.

For the first three molecules, interaction with Ser380 residue is well correlated to the first position of the molecules (Figure S7). Stabilizing interactions with the functional groups of the amino acid of the molecules can also explain this ranking. For instance, Lys306 and the CO_2^- group of the amino acid of the (*S)*-3-amino-tyrosine stay close during all the simulation. For the *(R)*-2,4-dihydroxyphenylalanine, Glu203 remains close with the NH_3^+ group of the amino acid (Figure S8). These interactions could prevent the exit of the molecules from the active site.

Since computational studies (docking and MD simulations) were performed on the *oxy* form of a homology model of TyH and the X-ray studies on Tyrp1, a direct comparison is not possible between the simulations and the crystallographic structures. Nevertheless, results can be correlated and linked to biological assays. Indeed, in line with the X-ray studies and biological assays, MD simulations confirm the lack of activity of the racemic form of the 3,5-dihydroxyphenylalanine, since both enantiomers after 60 ns leave the active site. In contrast, MD simulations highlight the high activity of *(S)*-3-amino-tyrosine. Regarding 2,4-dihydroxyphenylalanine, the situation is more intricate, as the two enantiomers show a different behaviour during the MD simulations. Given these results, along with the X-ray structure of Tyrp1 indicating an interaction with the active site, while biological assays on TyH with racemic mixture showing no activity, it seems important to obtain the two enantiomers and evaluate their individual activity against TyH. According to the MD studies, we anticipate that *(R)*-2,4-dihydroxyphenylalanine will exhibit activity, while *(S)*-2,4-dihydroxyphenylalanine is expected to be inactive.

2.5. Synthesis of Enantiopure 2,4-Dihydroxyphenylalanine

Our racemic synthesis route involving an azlactone (Scheme 2) led us to consider a synthetic variation allowing the separation of the 2,4-dihydroxyphenylalanine enantiomers *via* the formation of diastereomers obtained in the second step (Scheme 3). For this purpose, azlactone (**2b**) was reacted with (*S*)-methylbenzylamine as an enantiopure chiral copula, leading to the opening of the heterocyclic part of (**2b**) and to the formation of (**8**) in 70% yield. The hydrogenation of the benzylidene moiety with H_2 over Pd/C catalyst is quantitative and drove to the clean formation of the diastereomers (**9b**) and (**9b'**). Their separation was then carried out by dissolving the mixture almost completely in hot ethyl acetate: the recovered insoluble part consisted in (**9b**) while the second diastereomer (**9b'**) crystallized gradually in the filtrate which cools. We did not try to

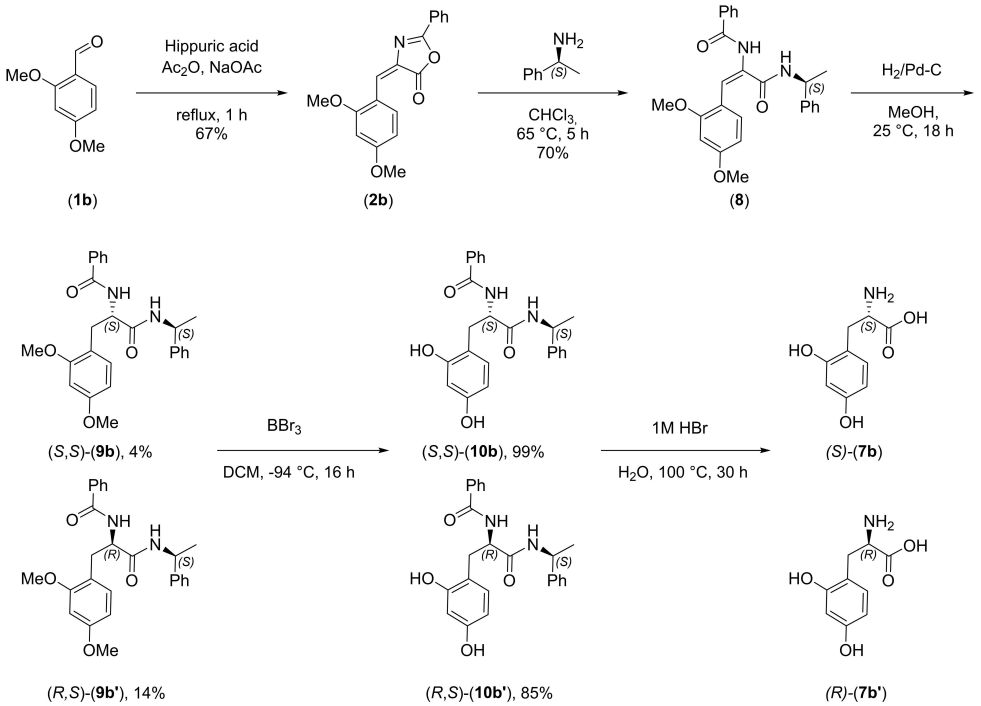

Scheme 3. Synthesis of enantiopure 2,4-dihydroxyphenylalanine

Table 3. MM/GBSA results extracted for a long simulation of 100 ns and from ten independent simulations of 10 ns.

Molecules	$\Delta G_{binding}$ (kcal/mol, 100 ns)	$\Delta G_{binding}$ (kcal/mol, 10 ns)
(R)-2,4-dihydroxyphenylalanine	-3 ± 3	not done
(S)-3-amino-tyrosine	-7 ± 3	-8 ± 3
L–DOPA	-13 ± 2	-11 ± 2
(S)-3-iminoquinone-tyrosine	-14 ± 3	-15 ± 3

optimize the yield by having enough separated compounds to continue the synthesis. Crystals of (**9b'**) were suitable for X-ray analysis and knowing the (*S)* configuration of the chiral copula, the complete configuration of (**9b'**) could be assigned to be (*R,S*) (Figure S9, see SI for details). Thus the other diastereomer (**9b**) has the (*S,S*) configuration. Following steps are similar to those developed in the previous synthesis, the phenols are deprotected with BBr_3 to (**10b**) and (**10b'**) and then a final hydrolysis with 1 M HBr removes the chiral copula. The absolute value of optical rotations in water of (+)-(*S*)-(**7b**) ($[\alpha]_D^{20} = +28.3°$) and (−)-(*R*)-(**7b'**) ($[\alpha]_D^{20} = -26.9°$) are close assuming that no racemization occurs during the final deprotection step.

Then biological assays were performed but no inhibition activity was observed for both enantiomers. To get more insights in relation with these results in relation with those of the MD simulations, molecular mechanics energies combined with the generalized Born and surface area continuum solvation (MM/GBSA method)[48] were performed.

2.6. MM/GBSA Free Energy Calculations

MM/GBSA method is a popular approach to rationalize observed differences of activities for small ligands to biological macromolecules with a modest computational effort.[49] It has been applied to a large number of systems with success. In MM/GBSA, the free energy of binding a molecule with its receptor is given by the relation (Eq. 3):

$$\Delta G_{binding} = \langle G_{complex} \rangle - \langle G_{ligand} \rangle - \langle G_{Protein} \rangle \quad (3)$$

Each component is expressed according to the equation (Eq. 4)

$$G = E_{bnd} + E_{el} + E_{vdw} + G_{pol} + G_{np} - TS \quad (4)$$

where the first three terms are standard MM energy terms from bonded, electrostatic and Van der Waals interactions. Gpol and Gnp are the polar and non-polar contributions to the solvation free energies, obtained for Gpol by using the generalized Born (GB) model whereas the non-polar term is estimated from a linear relation to the solvent accessible surface area (SASA).

Calculations were performed on the *(S)*-3-amino-tyrosine and the (*R)*-2,4-dihydroxyphenylalanine and compared to the *L*–DOPA in order to understand the results from the biological assays. Given the similar size of the three molecules, the last term, i.e. entropy multiplied by the absolute temperature, was not evaluated. Initially, we used the MD simulation of 100 ns and extracted 30 snapshots between 10 and 40 ns since the molecules bind well to the active site in this interval. Then, to reduce standard deviation and the uncertainty in the results due to a single long simulation,[49] ten independent simulations of 10 ns were used. The results are listed in Table 3, with the detail of all values of the GBSA equation in supporting information (Table S1, figure S10).

Based on the MM/GBSA values, *(S)*-3-amino-tyrosine ($\Delta G_{binding} = -7\pm3$ kcal/mol) and *(R)*-2,4-dihydroxyphenylalanine ($\Delta G_{binding} = -3\pm3$ kcal/mol) should interact with lower affinity than *L*–DOPA. In fact, their $\Delta G_{binding}$ are greater than that of *L*–DOPA ($\Delta G = -13\pm2$ kcal/mol). The same conclusion was obtained for the *(S)*-3-amino-tyrosine when we used ten independent simulations of 10 ns.

These results are in agreement with the biological assays for the *(R)*-2,4-dihydroxyphenylalanine but not for the *(S)*-3-amino-tyrosine, which show inhibitory activity of the diphenolase activity of TyH. The resulting values on the *(S)*-3-amino-tyrosine therefore led us to make a new hypothesis. Since *(S)*-3-amino-tyrosine has an oxidizable group, it would react as a substrate with the enzyme to form an iminoquinone[50,51] and the product of the oxidation reaction would inhibit the enzyme (Scheme 4). To support this hypothesis, a computational study was carried out on this product, hereafter named 3-iminoquinone-tyrosine (**11**).

We performed docking study on this molecule. The molecule also displayed a high affinity binding to the active site, with a hydrogen bond between the NH group of the 3-iminoquinone-tyrosine and the peroxo group. This hydrogen bond is maintained during all the MD simulations (Figure S11, S12). Results of MM/GBSA calculations are given in Table 3. Values of $\Delta G_{binding}$ obtained for the 3-iminoquinone-tyrosine (**11**) form were always lower than those of *L*–DOPA. Based on these results, this molecule should therefore interact with the active site at higher affinity than *L*–DOPA, which could explain the biological tests and would validate our hypothesis. To verify

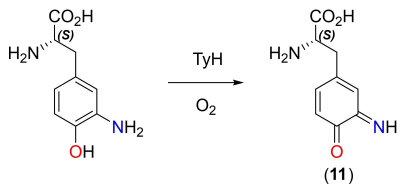

Scheme 4. Oxidation of (*S*)-3-amino-tyrosine into a (*S*)-3-iminoquinone-tyrosine (**11**) by TyH.

this, we trialled to obtain (**11**) in a pure form. Attempts with several reagents to oxidize (*S*)-3-amino-tyrosine (electrochemical oxidation, oxidation under O_2 atmosphere, use of various oxidant *i.e* silver salts, $NOBF_4$, $NaIO_4$) did not lead to the isolation of the expected iminoquinone (**11**). The major compound formed in the medium was phenoxazine (**13**), identified by mass spectrometry (Figure S13 "full spectrum"). Its appearance is only consistent with the subsequent formation of iminoquinone (**11**), which hydrolyses rapidly to the *L*-dopaquinone (**12**). These last two compounds were also detected by mass spectrometry in the reaction mixture, although in smaller quantities (Figure S9 "MS magnification"). It is known that quinones are very unstable electrophilic compounds that react rapidly with the nucleophiles present. In our case, the nucleophile is 3-amino-tyrosine, which has not yet oxidized (also visible in the spectrum) and forms a cyclocondensation product (**13**) with *L*-dopaquinone (**12**). These findings are in agreement with the work of Washington et al.[43] on the oxidative condensation of 2-amino-phenol (a compound very close to 3-amino-tyrosine) to 2-aminophenoxazin-2-one. However, this reactivity remains compatible with our hypothesis that for (*S*)-3-amino-tyrosine the iminoquinone (**11**) should be the true inhibitor of TyH. Indeed, (**11**) is well fixed in the active site of TyH, as shown by MD simulations, and thus reacts less to form (**12**) and (**13**) (Scheme 5).

Similarly, we could envisage an oxidation of 2,4-dihydroxyphenylalanine to produce, as the last product, two quinones (Scheme 6). Docking and MD simulations were also performed on the two products but in this case, they leave the active site from the beginning of the MD simulation (Figure S14). This result could also explain the lack of activity observed for the 2,4-dihydroxyphenylalanine in biological assays.

Taken together, docking studies, X-ray structural analyses with the non-redox Tyrp1 and molecular dynamics give us a strong indication that the molecules have high affinity for the active site of TyH. Further biological assays combined with MM/GBSA free energy calculations suggest that to understand the activity of these molecules on TyH, we have to also analyse the oxidation reaction products of these molecules.

3. Conclusions

Our study shows how combined experimental and computational studies provide a better understanding of human tyrosinase inhibition. We synthesized and evaluated three derivatives of a phenylalanine-derived compound. The racemic forms of 3,5- and 2,4 -dihydroxyphenylalanine have been synthetized in 7 steps starting from the corresponding dihydroxybenzaldehydes.

No particular activity was observed for the racemic form of 3,5-dihydroxyphenylalanine when testing against the diphenolase activity of TyH. This is in line with X-ray studies carried out with Tyrp1, a non-redox TyH homolog with zinc instead of copper ions in the active site. Tyrp1 crystals soaked with 3,5-dihydroxyphenylalanine shows no molecule inside the active site, which correlates with molecular dynamics using a TyH model, where both enantiomers leave the active site after 60 ns.

On the other hand, we obtained the X-ray structure of the racemic form of 2,4-dihydroxyphenylalanine with Tyrp1, which indicates an interaction of the molecule within the active site of TyH. Molecular dynamics confirms this interaction for the *(R)* enantiomer of the molecule. Then to go further on the activity

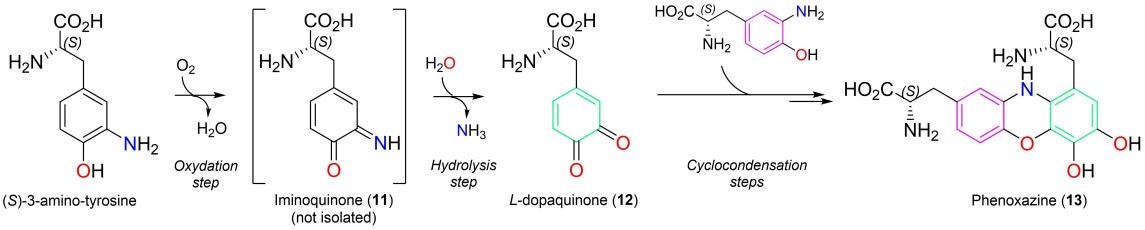

Scheme 5. Oxidative condensation of (*S*)-3-amino-tyrosine *via* iminoquinone (**11**) and *L*-dopaquinone (**12**) in phenoxazine (**13**).

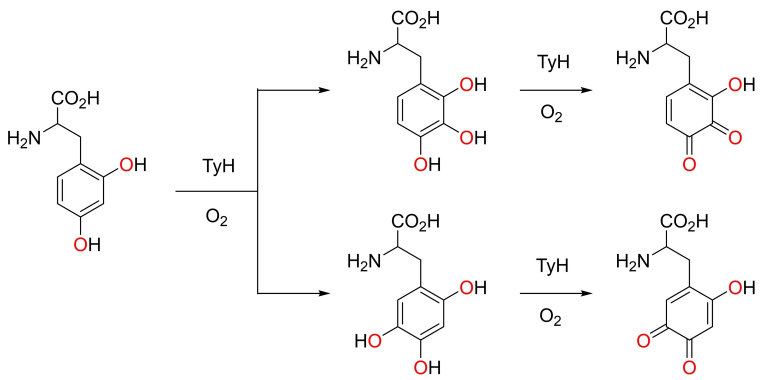

Scheme 6. Possible oxidation form of 2,4-dihydroxyphenylalanine by TyH.

of 2,4-dihydroxyphenylalanine, new synthesis of both enantiomers has been performed in 5 steps, including enantiomer separations of a protected intermediates. However, even after deracemization of the molecule, biological activity assays show no diphenolase activity of TyH, including (*R)* enantiomer. Free binding energies calculations using the MM/GBSA method support these results, with value of $\Delta G_{binding}$ greater than each of the natural substrate.

Finally, (*S*)-3-amino-*L*-tyrosine shows inhibition activity with isolated TyH ($K_{IC} = 0.10 \pm 0.02$ mM and $K_{IU} = 0.09 \pm 0.08$ mM), melanoma cell lysates ($IC_{50} = 0.08 \pm 0.01$ mM), and entire cells (50% of activity inhibition at 1 mM of *(S)*-3-amino-tyrosine). An X-ray structure of the Tyrp1-compound complex was also obtained, even if the value of $\Delta G_{binding}$ using MM/GBSA calculations keeps greater than each of the natural substrate. To explain the inhibition mechanism of this molecule, we suggest that a first oxidation of the molecule is required to give a (*S*)-3-iminoquinone-*L*-tyrosine. MM/GBSA calculations confirm the inhibition of TyH by this molecule.

Collectively, this study demonstrates that the integration of experimental and computational studies offers a new perspective on the intricate landscape of human tyrosinase inhibition.

Experimental Section

Docking Studies

Docking calculations were performed using Autodock 4.2 software.[38] For TyH, we used a homology model of TyH based on the crystallographic structure of Tyrp1 (PDB: 5 M8P).[10] This choice is governed by the fact that this enzyme shares 70% of similarity with TyH and also exhibits good interaction with known substrates of TyH,[10] even if TyH contains a dicopper site (in place of the dinuclear zinc site of 5 M8P). We have already used this model in a previous publication[36] and showed is high degree of similarity with the one obtained with the AlphaFold AI approach[37] (AF—P14679-F1 model_v2). The model is taken in its oxy form since it is the active form in the mono and diphenolase activities and the molecules tested can interact with both activities. Polar hydrogen atoms and Kollman charges were added to the protein using AutoDock Tools 1.5.6.[52] This tool aims to generate protonation states reasonable at physiological pH. Only the protonation state for histidine residues are changed, in histidine neutral ε-protonated for all the histidines, and in histidine neutral δ-protonated for the histidines coordinated to copper atoms of TyH. The"AD4_parameters.dat" file in Autodock[38] was edited manually to include Cu ion parameters (an arbitrary charge of +2, Rii = 3.50 Å, ep-sii = 0.005 kcal/mol and vol = 12 $AÅ^3$). The geometries of the molecules were optimized using the B3LYP functional in combination with the set of base 6–311 + G (d, p) for all atoms with the Gaussian16 software.[53] Vibration frequency calculations were performed to ensure that each geometric optimization converges to an actual minimum and the effect of the solvent was taken into account in geometric optimizations with the IEFPCM formalism. The solvent used was water. Gasteiger charges were added to the molecules using AutoDock Tools 1.5.6. A grid of 80×80×80 points centered on the coordinates of one copper atom of the active site and separated by 0.2 Å was used for the docking. A conformational search was performed using a genetic algorithm with an initial population of 300 randomly placed individuals, a maximum number of 2.5×105 energy evaluations, a maximum number of 2.7×104 generations, a mutation rate of 0.02, and a crossover rate of 0.8. One hundred different conformers of the molecules were generated and the energy values of conformers were reported as a histogram. The best rank position is taken as the docked position. With the same procedure, using parameters of zinc instead of copper in the "AD4_parameters.dat" file of Autodock, we docked the *L*-Tyrosine into Tyrp1. We used the crystal structure of Tyrp1 in complex with the *L*-tyrosine (5 M8P) and removed the *L*-Tyrosine. The re-docked *L*-tyrosine is superimposed to the co-crystallized *L*-tyrosine, exhibiting the same interactions with the active site and validating the procedure.

Molecular Dynamics (MD)

MD were performed with AMBER18 software[54] under periodic boundary conditions. The structures of the complexes obtained after docking are placed in a rectangular water box containing water molecules and the tip3p force field.[55] For the protein, the force field ff14sb[56] was used with specific parameters for copper atoms, histidines and the peroxo group of the active site as it was described in our previous publication.[57] For the ligands, the parameters are generated using Amber's Antechamber program with the GAFF force fields and the charges were obtained by the RESP approach after a calculation with Gaussian16 software[48] of the electrostatic potential at the HF / 6–31 g* level. The size of the rectangular water box is chosen to be 10 Å larger than the solute in all directions. Sodium cations are added as necessary to neutralize the system and long-range electrostatic interactions are simulated using the Ewald particle mesh method with a cut-off value of 10 Å. First 5000 cycles of minimization in the NTV assembly is achieved on the whole system to remove steric overlaps. Restraints with a force constant of 500 $kcal.mol^{-1}.Å^{-1}$ are added during the minimization on the positions of copper atoms, histidines and the peroxo group of the active site. Then heating in the NTV assembly from 0 K to 300 K is performed with the same restraint on the active site for 0,5 ns followed by 0,5 ns of simulation with a target temperature of 300 K in reducing the force constant at 250 $kcal.mol^{-1}.Å^{-1}$. To control the temperature, we used the Langevin thermostat with a value of the collision frequency equals to 2. Same values of the collision frequency and of the force constant were used to the production run in the NPT assembly for 100 ns. We used constant pressure periodic boundary with an average pressure of 1,01325 bar and a pressure relaxation time of 2 ps. During the 100 ns of MD simulation, the shake algorithm is used so the time step was 2 fs. The nonbonded cut-off was 10 Å. To evaluate the deviation during the 100 ns of MD simulation, rmsd analysis from the initial structure was performed in taking account only the residues of the protein without its hydrogen atoms using cptraj software.[58] Plots are given in supporting information (Figure S5). For the ligand and its binding pose, a characteristic distance between the active site and an atom of the ligand is plotted in Figure6. To confirm our results on the best ligands, the (S) 3-amino-tyrosine and the product of its oxidation reaction, MD simulations were performed in triplicate. Plots of the characteristic distance of their binding poses and rmsd analysis are given in supporting information (Figure S6, S12).

MM/GBSA Calculations

Calculations are carried out on various positions obtained after different dynamics using the perl script mmpbsa.pl associated with

the AMBER18 software[54] The atomic radii developed by Onufriev and coworkers (Amber input parameter igb = 2) are chosen for all GB calculations.[59] Since parameters are not defined for copper atoms into the sander program, we modify the type of copper atoms in the prmtop file into the type of the defined ion Mg^{2+}. Copper atoms are not directly involved in the interaction with the ligand and their positions are close for all structures since they are restrained during the MD simulations. So same errors are introduced in our calculations with this substitution and the comparison of the MMGBSA calculations can be done. The nonpolar solvation energy was calculated in using solvent accessible surface (SASA) with the surface tension parameter $\gamma = 0.0227$ kJ/mol/Å^2 and a parameterized value b = 3.85 kJ/mol. The binding energy (ΔG) is calculated according to the equations (3) and (4) of the part "Results and Discussion" and all the terms are added in supporting information (Table S1).

Two procedures are used. For the simulation of 100 ns, every 5 structure was been extracted from the trajectory between the 50th and the 200th structures, an interval in which the binding pose is stable (Figure6). Analysis of the rmsd deviation on this interval in taking account all the protein and the ligand (FigureS10 A) confirms the validity of this interval to perform MMGBSA calculations. For calculations with the ten simulations, ten structures were automatically extracted between 2 and 4 ns and an average of the ten MMGBSA calculations were done. Values of the rmsd deviation between all the frames of this interval were also added (figure S10B).

X-ray Crystallography Analyses

Recombinant Human Tyrp1 Expression and Purification

Overexpression and purification of the human intramelanosomal domain of hTyrp1 (residues 25 to 471) respectively were done according to already published procedures.[10] A final purification step was applied to Superdex200 10/300 GL (Cytiva) column pre-equilibrated with gel filtration buffer (10 mM Tris-HCl, pH 7.8, 100 mM NaCl) for further purification at room temperature. Tyrp1 protein-containing peaks were pooled and concentrated using a centrifugal filter unit (Amicon® Ultra-4, 3.5 kDa MWCO) to around 30 mg/mL. Concentrated proteins were flash-frozen using liquid nitrogen and stored at −80 °C, ready to be used for crystallization or other downstream experiments.

Protein Crystallization

Crystallization plates for Tyrp1 were set up manually following previously identified crystallizing condition ((6–16) % PEG 6000, (1.5–3.0) mM zinc chloride, 100 mM Tris-HCl pH 8.0). Tyrp1 crystals were grown in hanging drops at 4 °C through vapour diffusion method at 1 : 1 protein:reservoir ratio (2 μL final volume). A total number of three compounds, namely racemic 2,4-dihydroxyphenylalanine, 3,5-dihydroxyphenylalanine and (*S*)-3-amino-tyrosine were tested in this study for binding experiments. For soaking experiments, compounds were introduced to fully grown Tyrp1 crystals for varying time (up to 8 minutes), followed by quick cryo-protection by cryo-protectant (12 % PEG 6000, 2.5 mM ZnCl2, 0.1 M Tris pH 8.0, 20 % Glycerol) before cryo-cooled in liquid nitrogen. As for co-crystallization experiment, screening plates were set up through the HTX crystallization facility (EMBL, Grenoble, France). Co-crystallization screening plates for Tyrp1 protein with (*S*)-3-amino-tyrosine were set up at 4 °C at 1 : 1 protein-compound: reservoir ratio (300 nL final volume) with two protein:compound ratios (1 : 2 and 1 : 4). Compound-bound co-crystal was obtained via sitting-drop vapour diffusion method after a month.

X-ray Diffraction Data Collection, Processing and Refinement

Crystallographic data were collected at 100 K at the ESRF beamlines ID23-2,[44] MASSIF-3 (ID30 A-3)[45] and ID30B[46] for compound-soaked Tyrp1 crystals, and at ESRF beamline MASSIF-1 (ID30 A-1)[47] for Tyrp1-compound co-crystal. Data collection were aided by beamline-control GUI MxCuBE.[60] X-ray datasets were processed using the program XDS and then scaled and integrated using Collaborative Computational Project, Number 4 (CCP4) software suite.[61] Structure determination was carried out by molecular replacement using *MOLREP* and MoRDa (from the CCP4 package) or *PHASER*, integrated in the Python-based Hierarchical ENvironment for Integrated Xtallography (*PHENIX*).[62] Subsequent refinement was carried out using REFMAC (CCP4) and PHENIX. Further manual model rebuilding and refinement were iteratively performed with *COOT*[63] and *PHENIX* respectively. Crystallographic Information File (CIF) for compounds used were generated using electronic Ligand Builder and Optimization Workbench (*eLBOW*) available through *PHENIX*.

X-ray energy Scanning and Single-Wavelength Anomalous Dispersion (SAD)

Energy scanning and single-wavelength anomalous dispersion (SAD) experiments were performed on one compound-soaked Tyrp1 crystal for Tyrp1 metal identification. Energy scanning at Zn-edge (9.659 keV) and Cu-edge (8.979 keV) were performed on one compound-soaked Tyrp1 crystal. Following that, different set of x-ray diffraction data were collected below and above Zn-edge to allow for anomalous difference Fourier map calculation.

X-Ray Fluorescence Data Collection and Processing

X-ray fluorescence (XRF) emission spectra was collected at the ESRF beamline ID30B with 14.0 keV incident beam at 0.3 % transmission over 10-second exposure time. This measurement was done on 2,4-dihydroxyphenylalanine soaked Tyrp1 crystals. Following data collection, XRF emission spectra were visualized and analyzed using Python multichannel analyzer (PyMCA) integrated in MxCuBE.[60]

Biological Activity Assays

General: L–Dopa, 3-amino-tyrosine and pure melanin are available from Sigma-Aldrich. The ViaLight™ Plus kit was purchased from Fisher Scientific.

Enzymatic assays on purified enzyme. TyH was produced and purified as previously described.[40] TyH diphenolase activity was spectrophotometrically monitored at 25 °C by following the formation of dopachrome at a wavelength of 475 nm (ε = 3,400 $M^{-1}.cm^{-1}$).[64] *L*–DOPA was dissolved in phosphate buffer saline (PBS) 100 mM, pH 7.0. Inhibitors were dissolved in PBS. The concentrations of *L*–DOPA employed ranged from 0.096 mM to 9.6 mM for kinetic assay and was fixed to 2.4 mM for the diphenolase activity. The concentrations of inhibitors tested ranged from 0.04 to 1 mM. The IC_{50} and the kinetic constants were determined in a 96-well plate assay, using a SpectraMax 190 Absorbance Microplate Reader equipped with SoftMax 4.8 software. The K_M and V_M values were calculated as described in the manuscript by fitting the obtained V_i to the Michaelis-Menten equation, using the software KaleidaGraph. The type of inhibitory mechanism against Ty during the oxidation of *L*–DOPA was

determined by fitting the V_0 values obtained at different substrate and inhibitor concentrations to the equations (Eq. 1 and Eq. 2) describing different modes of inhibition. All measurements were done in triplicate, and the reported values are the mean and the standard error of at least three independent experiments.

Cell lysates: Human melanoma cells (MNT-1) were obtained from the National Institute of Health (NIH) and were grown in Dulbecco's Modified Eagle Medium (DMEM) supplemented with 10% fetal calf serum and 1% antibiotics, in 75 cm^2 ventilated flask maintained at 37 °C in a 5% CO_2 incubator. Cells were routinely passed using trypsin-EDTA solution. Inhibition of tyrosinase by test compounds was first evaluated using cell lysate prepared from MNT-1 cells. Briefly, confluent MNT-1 cells cultivated on 75 cm^2 flasks were washed with PBS and detached using trypsin-EDTA solution. Cells suspension was aliquoted in cryotubes (approximately 4.10E6 cells per tube) and tubes were then centrifuged at 1,200 rpm for 5 min. Supernatants were eliminated and cells pellets were snapfrozen in liquid nitrogen before being stored at −80 °C until tyrosinase assay. The day of the assay, tubes containing cell pellets were defrosted and cells were resuspended in 1.5 mL of PBS containing 0.1% Triton X-100. Tubes were incubated in ice during 10 min before being centrifuged at 1,200 rpm for 5 min. Supernatants corresponding to MNT-1 cell extract were collected and used for tyrosinase assay. Cell extracts were first diluted to 10 mL with PBS and then added to 96-wells plate (100 μL per well). 4 μL of test compounds (diluted in PBS) were next added to the wells and were serially diluted 2-times directly into the 96-wells plate. Finally, 100 μL of a *L*–DOPA solution (initial concentration of 4.8 mM) were added in each well and the OD at 475 nm was immediately recorded (t_0 measurement). Plates were then incubated at 37 °C, OD at 475 nm being continuously recorded until it reached OD ≈0.5 (about $tf = t_0 + 3$ hours). Variation of $OD_{600\ nm}$ was calculated (OD (t_f)–OD (t0)) and used to determine IC_{50}.

Whole cells: Inhibition of tyrosinase activity by test compound was also conducted using whole cells. Briefly, MNT-1 cells grown on 75 cm^2 flask were detached using trypsin-EDTA solution. Detached cells were then placed onto 6-wells plates at the initial density of $2{,}7\times10^5$ cells per cm^2 and incubated at 37 °C in a 5% CO_2 incubator. After two to three days, when confluence was reached, cell medium was changed to fresh medium and MNT-1 cells were treated with increasing concentrations of test compound (dissolved in PBS, concentration range from 0.5 to 2 mM) all wells (including negative controls) receiving the same amount of vehicle. Cells were then incubated for 96 h at 37 °C in a 5% CO_2 incubator. At the end of the incubation, cells were washed three times with cold PBS and were then transferred to Eppendorf tubes. After centrifugation (at 1,200 rpm for 5 min), cell pellets were finally lysed by adding 0.5 mL of 0.1% Triton X-100. The procedure is then the same as for the lysate, except that the inhibitors is not added in the wells, only the cell pellet and *L*–DOPA.

Cytotoxicity assays: DL_{50} was determined using whole cells and the ViaLight™ plus kit. Briefly, MNT-1 cells grown on 75 cm^2 flask were detached using trypsin-EDTA solution. Detached cells were then placed onto 6-wells plates at the initial density of 2.7 10^5 and incubated at 37 °C in a 5% CO_2 incubator. After two to three days, when confluence was reached, cell medium was changed to fresh medium and MNT-1 cells were treated with increasing concentrations of test compounds (dissolved in PBS) all wells (including negative controls) receiving the same amount of vehicle. The concentrations of inhibitor tested ranged from 0.5 to 12 mM. Cells were then incubated for 48 h at 37 °C in a 5% CO_2 incubator. At the end of the incubation, cell medium was removed and cells were washed three times with cold PBS. 35 μL of cell medium was added in each well, followed by NaOH 1 M. After 10 min, 50 μl of AMR (ATP monitoring reagent) reagent was added. After 2 min, luminescence was monitored. The value of each well was then compared to a witness well containing only cells without test compounds.

Chemical Synthesis

General: All starting materials and reagents commercially available (Sigma-Aldrich Milan, Italy; Alfa Aesar Karlsruhe, Germany) were used without further purification. Solvents were purified by standard methods before use. The silica gel used for the chromatographic columns is supplied by Merck, with a diameter of 40–63 μM for flash columns or 15–40 μM for DCVCs. Analytical thin layer chromatographies (TLC) were carried out on plates pre-coated with silica gel Merck 60 F254 (250 μm thick). ESI mass spectra were recorded on an Esquire 300 plus Bruker. Semi-preparative HPLC separations were performed on a Gilson-322-pump apparatus equipped with a Gilson-156 detector (detection at 260 nm and 280 nm) and a Nucleosil® column (C18; 10 mm diameter/250 mm length; 7μm particle size and 100 Å porosity; flow rate of 4 mL/min; injected volume 1 mL); the mobile phase consists of eluents A (H_2O/ triethylamine/acetonitrile = 92.5/2.5/5) and B (H_2O/ acetonitrile = 5/95) with the following gradient: 0–2 min, 0% B then 2–14 min, 0%-50% B and finally 14–15 min, 50%-0% B. High resolution masses (HRMS) were recorded on a Waters Xevo G2-S QTof device. ^{1}H NMR spectra were recorded on a Bruker Avance III 400 (^{1}H at 400 MHz,^{13}C at 100 MHz) or 500 (^{1}H at 400 MHz,^{13}C at 125 MHz) at 323 K with the deuterated solvent as a lock.

(1 b) 2,4-dimethoxybenzaldehyde,[35] $C_9H_{10}O_3$ (166.06 g/mol). Protocol: 5.00 g of 2,4-dihydroxybenzaldehyde (36 mmol, 1 eq) and 10.12 g of K_2CO_3 (90 mmol, 2.5 eq) are introduced into a 100 mL flask and dissolved in 25 mL of acetone. Then, 5.6 mL of methyl iodide (90 mmol, 2.5 eq) are added to the mixture dropwise. The solution heated at reflux overnight. Then, filtration is performed to remove excess of K_2CO_3. The filtrate is evaporated and the product is obtained without further purification in the form of a pinkish-white solid (5.09 g, 85%). ^{1}H NMR (400 MHz, chloroform-*d*): δ = 10.30 (s, 1H, aldehyde), 7.83 (d, J = 8.8 Hz, 1H), 6.54 (d, J = 8.8 Hz, 1H), 6.47 (s, 1H), 3.92 (s, 3H), 3.89 (s, 3H) ppm. ^{13}C NMR (126 MHz, chloroform-*d*): δ = 188.3, 166.2, 163.2, 130.8, 119.1, 105.7, 97.9, 55.6, 55.6 ppm. MS (ESI) *m/z:* calcd for $C_9H_{10}O_3Na^+$ = 189.06, found = 188.87 $[M+Na]^+$.

(2 a) 4-(3,5-dimethoxybenzylidene)-2-phenyl-5(*4H*)-oxazolone, $C_{18}H_{15}NO_4$ (309.10 g/mol). In a 100 mL flask fitted with a magnetic bar, 5.00 g of commercially 3,5-dimethoxybenzaldehyde (30 mmol, 1.0 eq), 5.91 g of hippuric acid (33 mmol, 1.1 eq) and 1.72 g of sodium acetate (21 mmol, 0.7 eq) are heated to reflux with stirring for 1 hour in 15 mL of acetic anhydride. A solid formed when the mixture cools. After filtration and recrystallization in isopropyl ether, the desired product is obtained (7.55 g, 82%).^{1}H NMR (400 MHz, Chloroform-*d*): δ = 8.18 (d, J = 7.8 Hz, 2H), 7.64–7.62 (m, 1H), 7.57–7.54 (m, 2H), 7.44 (s, 2H), 7.20 (s, 1H), 6.61 (s, 1H, benzylidene), 3.91 (s, 6H) ppm. ^{13}C NMR (126 MHz, Chloroform-*d*): δ = 167.5, 163.6, 160.8 (2 C), 135.0, 133.5, 133.4, 131.75, 128.9 (2 C), 128.3 (2 C), 125.5, 110.1 (2 C), 109.9, 104.1, 55.4 (2 C) ppm. MS (ESI) *m/z:* calcd for $C_{18}H_{15}NO_4H^+$ = 310.10, found = 310.17 $[M+H]^+$, 342.19 $[M+Na]^+$, 364.18 $[M+K]^+$. M.p (°C): 136–138.

(2 b) 4-(2,4-dimethoxybenzylidene)-2-phenyl-5(*4H*)-oxazolone, $C_{18}H_{15}NO_4$ (309.10 g/mol). In a 100 mL flask fitted with a magnetic bar, 4.48 g of 2,4-dimethoxybenzaldehyde **1 b** (27 mmol, 1.0 eq), 5.32 g of hippuric acid (33 mmol, 1.1 eq) and 1.55 g of sodium acetate (19 mmol, 0.6 eq) are heated to reflux with stirring for 1 hour in 15 mL of acetic anhydride. A solid formed when the mixture cools. The product is obtained as a white solid without further purification (4.41 g, 50%).^{1}H NMR (400 MHz, Chloroform-*d*):

δ = 8.92 (d, J = 8.9 Hz, 1H), 8.18 (d, J = 7.2 Hz, 2H), 7.83 (s, 1H, benzylidene), 7.60–7.55 (m, 1H), 7.53–7.49 (m, 2H), 6.68 (dd, J_1 = 2.4 Hz, J_2 = 8.9 Hz, 1H), 6.47 (d, J = 2.4 Hz, 1H), 3.92 (s, 6H) ppm. ^{13}C NMR (126 MHz, Chloroform-*d*): δ = 168.3, 164.1, 161.9, 161.2, 134.6, 132.7, 130.2, 138.8, 128.8, 128.0, 126.2, 126.1, 116.2, 106.3, 97.7, 55.7, 55.6, 26.9 ppm. MS (ESI) *m/z:* calcd for $C_{18}H_{15}NO_4H^+$ = 310.10, found = 310.1 $[M+H]^+$, 332.1 $[M+Na]^+$, 348.08 $[M+K]^+$. M.p (°C): 152–153.

(3 a) Methyl 2-benzamido-3-(3,5-dimethoxyphenyl)-acrylate, $C_{19}H_{19}NO_5$ (341.13 g/mol). To a solution of 7.46 g of azlactone **2 a** (24 mmol, 1.0 eq) in 25 mL of dry MeOH is added NaOMe (48 mmol, 2 eq). The mixture is heated to 40 °C for 2 h with stirring. Water and a 1 M HCl solution are added to the mixture until a white solid precipitate. The solid is filtered off and rinsed with water. The pure product is obtained without further purification in the form of a white solid (7.64 g, quant.).^{1}H NMR (400 MHz, chloroform-*d*): δ = 7.89 (d, J = 7.7 Hz, 2H), 7.71 (s, NH), 7.60–7.56 (m, 1H), 7.51–7.48 (s, 2H), 7.36 (s, 1H, benzylidene), 6.68 (s, 2H), 6.39 (s, 1H), 3.89 (s, 3H), 3.67 (s, 6H) ppm. ^{13}C NMR (126 MHz, chloroform-*d*): δ = 165.7, 160.7 (2 C), 135.5, 133.5, 132.3, 131.4, 128.8 (2 C), 127.4 (2 C), 124.7, 107.3 (2 C), 102.1, 77.2, 77.0, 76.7, 55.2 (2 C), 52.8 ppm. MS (ESI) *m/z:* calcd for $C_{19}H_{19}NO_5H^+$ = 342.13, found = 342.19 $[M+H]^+$, 340.04 $[M–H]^-$. M.p (°C): 130–131.

(3 b) Methyl 2-benzamido-3-(2,4-dimethoxyphenyl)-acrylate, $C_{19}H_{19}NO_5$ (341.13 g/mol). To a solution of 4.42 g of azlactone **2 b** (1.1 mmol, 1.0 eq) in 15 mL of MeOH, is added MeONa (2.2 mmol, 2 eq). The mixture is heated to 40 °C for 2 h with stirring. Water and a 1 M HCl solution are added to the mixture until a white solid precipitate. The solid is filtered off and rinsed with water. The pure product is obtained without further purification in the form of a yellow solid (4.49 g, quant.).^{1}H NMR (400 MHz, chloroform-*d*): δ = 8.05 (s, NH), 7.87 (d, J = 7.4 Hz, 2H), 7.59 (s, 1H, benzylidene), 7.59 – 7.54 (m, 1H), 7.48–7.42 (m, 3H), 6.50 (m, 2H), 3.91 (s, 3H), 3.88 (s, 3H), 3.82 (s, 3H) ppm. ^{13}C NMR (126 MHz, chloroform-*d*): δ = 166.08, 162.00, 158.47, 133.96, 131.96, 131.09, 128.68, 128.6, 127.4, 127.4, 125.9, 123.5, 115.8, 105.3, 105.3, 98.7, 55.9, 55.4, 52.5 ppm. MS (ESI) *m/z:* calcd for $C_{19}H_{19}NO_5H^+$ = 342.13, found = 342.09 $[M+H]^+$, 364.06 $[M+Na]^+$. M.p (°C): 130–133.

***Rac*-(4 a) Methyl 2-benzamido-3-(3,5-dimethoxyphenyl)-propanoate**, $C_{19}H_{21}NO_5$ (343.13 g/mol). The reactant **3 a** (0.20 g,0.6 mmol) and 10 % by mass of Pd/C are introduced into a flask with 10 mL of MeOH and a drop of acetic acid. The vacuum is carried out before plugging a balloon filled with H_2 on the balloon. The mixture is heated to 40 °C overnight. The residual palladium is then filtered through Celite. The filtrate is collected and water is added. The pure product is obtained after extraction with ether, washing and drying as a white solid without further purification (0.21 g, quant.). ^{1}H NMR (400 MHz, chloroform-*d*): δ = 7.74 (d, J = 7.7 Hz, 2H), 7.51–7.49 (m, NH), 7.45–7.41 (m, 2H), 6.59 (d, J = 7.0 Hz, 1H), 6.36 (s, 1H), 6.28 (s, 2H), 5.10–5.05 (m, 1H), 3.79 (s, 3H), 3.72 (s, 6H), 3.27–3.16 (m, 2H) ppm. ^{13}C NMR (126 MHz, chloroform-*d*): δ = 171.9, 166.8 (2 C), 160.9, 138.0, 133.9, 131.8, 128.6 (2 C), 127.0 (2 C), 107.3 (2 C), 99.2, 77.2, 77.0, 76.7, 55.2 (2 C), 53.4, 52.4, 38.0 ppm. MS (ESI) *m/z*: calcd for $C_{19}H_{21}NO_5H^+$ = 344.13, found = 344.16 $[M+H]^+$, 341.97 $[M–H]^-$. M.p (°C): 102–103.

***Rac*-(4 b) Methyl 2-benzamido-3-(2,4-dimethoxyphenyl)-propanoate**, $C_{19}H_{21}NO_5$ (343.14 g/mol). The reactant **3 b** (1.00 g, 3.2 mmol) and 10 % by mass of Pd/C (0.25 g) are introduced into a flask with 25 mL of MeOH and a drop of acetic acid. The vacuum is carried out before plugging a balloon filled with H_2 on the balloon. The mixture is heated to 40 °C during two days. The residual palladium is then filtered through Celite. The filtrate is collected and water is added. The pure product is obtained after extraction with ether, washing and drying as a white solid without further purification (1.00 g, quant.). ^{1}H NMR (400 MHz, chloroform-*d*): δ = 7.63 (d, J = 7.2 Hz, 2H), 7.43–7.39 (m, 1H), 7.35–7.31 (m, 2H), 6.94 (s, 1H), 6.38–6.35 (m, 2H), 4.78 (q, J = 6.4 Hz, 1H), 3.73 (s, 3H), 3.71 (s, 3H), 3.67 (s, 3H), 3.10 (d, J = 6.4 Hz, 2H) ppm. ^{13}C NMR (126 MHz, chloroform-*d*): δ = 172.4, 167.0, 160.2, 158.3, 134.1, 131.7, 131.6, 128.5, 126.9, 116.9, 104.7, 98.7, 55.5, 55.3, 54.1, 52.2, 31.6 ppm. MS (ESI) *m/z:* calcd for $C_{19}H_{21}NO_5H^+$ = 344.14, found = 344.1 $[M+H]^+$, 366.1 $[M+Na]^+$. M.p (°C): 110–111.

***Rac*-(5 a) Methyl 2-benzamido-3-(3,5-dihydroxyphenyl)-propanoate**, $C_{17}H_{17}NO_5$ (315.11 g/mol). 0.30 g of compound **4 a** (0.8 mmol, 1 eq) is placed in a flask in a nitrogen/acetone bath (− 95 °C) and under an inert atmosphere. 2.74 mL of BBr_3 (8 eq) is added dropwise. The reaction is left to stir at room temperature overnight. The next day, the excess of BBr_3 is destroyed at 0 °C with MeOH. After evaporation, the mixture is taken up in water and the product of interest is extracted with CH_2Cl_2. The pure product is obtained after washing and drying as a yellow oil (0.25 g, quant.).^{1}H NMR (400 MHz, DMSO-d_6): δ = 9.00 (s, 2 OH), 8.63 (d, J = 7.7 Hz, NH), 7.81 (d, J = 7.7 Hz, 2H), 7.51–7.47 (m, 1H), 7.44–7.38 (m, 2H), 6.2 (s, 2H), 6.0 (s, 1H), 4.06–4.00 (m, 1H), 3.53 (s, 3H), 2.96–2.87 (m, 2H) ppm.

***Rac*-(5 b) Methyl 2-benzamido-3-(2,4-dihydroxyphenyl)-propanoate**, $C_{17}H_{17}NO_5$ (315.10 g/mol). To a flask cooled with a nitrogen/acetone bath (− 95 °C), under an inert atmosphere and containing 0.51 g of compound **4 b** (1.5 mmol, 1 eq), is carefully added 8 mL of BBr_3 (5.3 eq, 1 M in CH_2Cl_2). The reaction is left to stir at room temperature overnight. Then, the excess of BBr_3 is cautiously destroyed at 0 °C with MeOH. After evaporation, the mixture is taken up in water and the product of interest is extracted with CH_2Cl_2. The pure product is obtained after washing and drying as a white solid (0.35 g, 77 %).^{1}H NMR (500 MHz, DMSO-d_6): δ = 9.49 (s, OH), 9.07 (s, OH), 8.65 (d, J = 7.4 Hz, NH), 7.80 (d, J = 7.4 Hz, 2H), 7.54–5.52 (m, 1H), 7.48 - 7.45 (m, 2H), 6.90 (d, J = 8.2 Hz, 1H), 6.29 (d, J = 2.1 Hz, 1H), 6.10 (dd, J_1 = 8.2 Hz, J_2 = 2.1 Hz, 1H), 4.61 (dd, J_1 = 9.6 Hz, J_2 = 5.2 Hz, 1H), 3.61 (s, 3H), 3.05 (dd, J_1 = 13.5 Hz, J_2 = 5.2 Hz, 1H), 2.83 (dd, J_1 = 13.5 Hz, J_2 = 9.6 Hz, 1H) ppm. ^{13}C NMR (126 MHz, DMSO-d_6): δ = 211.8, 177.8, 171.6, 162.3, 161.2, 138.9, 136.7, 133.5, 132.5, 119.2, 111.2, 107.5, 58.4, 58.9, 36.2, 35.9 ppm. MS (ESI) *m/z:* calcd for $C_{17}H_{17}NO_5H^+$ = 315.10, found = 316.11 $[M+H]^+$, 329 $[M+Na]^+$, 338 $[M+K]^+$, 314 $[M–H]^-$. Anal.: calcd for = C (64.74 %), H (5.44 %), N (4.44 %); found = C (64.79 %), H (5.85 %), N (4.43 %). M.p (°C): 70.

***Rac*-(6 a) 2-benzamido-3-(3,5-dihydroxyphenyl)-propanoic acid**, $C_{16}H_{15}NO_5$ (301.10 g/mol). To 0.25 g of **5 a** (0.7 mmol, 1 eq) dissolved in a 10 mL THF: H_2O (5: 1) mixture, is added 0.05 g of LiOH (1.3 mmol, 3 eq). The mixture is left under stirring at ambient temperature overnight. The mixture is neutralized with a 1 M solution of HCl. The product is obtained after evaporation to dryness and extraction with ether as an orange oil without other purification (0.27 g, quant.).^{1}H NMR (500 MHz, DMSO-d_6): δ = 9.06 (s, 2 OH), 8.61 (d, J = 8.0 Hz, NH), 7.81 (d, J = 10.7 Hz, 2H), 7.54–7.51 (m, 1H), 7.46–7.44 (m, 2H), 6.15 (s, 2H), 6.02 (s, 1H), 4.53 (dd, J_1 = 11.6 Hz, J_2 = 4.5 Hz, 1H), 2.96 (dd, J_1 = 4.5 Hz, J_2 = 13.8 Hz, 1H), 2.87 (dd, J_1 = 11.6 Hz, J_2 = 13.8 Hz, 1H) ppm. ^{13}C NMR (126 MHz, DMSO-d_6): δ = 172.7, 170.8, 166.8, 158.6, 140.0, 134.2, 131.9, 128.7, 128.7, 127.9, 127.9, 107.5, 107.5, 101.3, 52.4, 31.1 ppm. MS (ESI) *m/z:* 301.98 $[M+H]^+$, 324.01 $[M+Na]^+$, 339.94 $[M+K]^+$, 299.94 $[M–H]^-$.

***Rac*-(6 b) 2-benzamido-3-(2,4-dihydroxyphenyl)-propanoic acid**, $C_{16}H_{15}NO_5$ (301.10 g/mol). To 0.09 g of **5 b** (0.28 mmol, 1 eq) dissolved in a 5 mL THF: H_2O (5: 1) mixture, is added 0.034 g of LiOH (0.84 mmol, 3 eq). The mixture is left under stirring at ambient temperature overnight. The mixture is neutralized with a 1 N solution of HCl. The product is obtained after evaporation to dryness and extraction with ether as an oil without other

purification (0.06 g, 74%). ^{1}H NMR (500 MHz, DMSO-d_6): δ = 9.46 (s, OH), 9.02 (s, OH), 8.48 (d, J = 7.7 Hz, NH), 7.81–7.75 (m, 2H), 7.56–7.50 (m, 1H), 7.46 (m, 2H), 6.92 (d, J = 8.2 Hz, 1H), 6.28 (d, J = 2.4 Hz, 1H), 6.10 (dd, J_1 = 8.2, J_2 = 2.4 Hz, 1H), 4.56 (ddd, J_1 = 10.2 Hz, J_2 = 7.7 Hz, J_3 = 4.4 Hz, 1H), 3.09 (dd, J_1 = 13.6 Hz, J_2 = 4.4 Hz, 1H), 2.81 (dd, J_1 = 13.6 Hz, J_2 = 10.2 Hz, 1H) ppm. ^{13}C NMR (126 MHz, DMSO-d_6): δ = 174.0, 166.6, 157.4, 156.4, 134.5, 131.8, 131.7, 128.7 (2 C), 127.6 (2 C), 114.9, 106.4, 102.7, 53.6, 31.3 ppm. MS (ESI) *m/z*: calcd for $C_{16}H_{15}NO_5H^+$ = 301.10, found = 302.05 $[M+H]^+$, 324.05 $[M+Na]^+$, 340.02 $[M+K]^+$.

***Rac*-(7 a) 3,5-dihydroxyphenylalanine**,[29] $C_9H_{11}NO_4$ (196.18 g/mol). Hydrolysis is performed by reacting 0.03 g of compound **6 a** in a 5 mL HBr solution (2 M). The reaction is refluxed overnight under an inert atmosphere. The solution is taken up in water and then the aqueous phase is washed with 3 x AcOEt and evaporated to dryness. The pure product is obtained after purification by HPLC as white powder (20%).^{1}H NMR (500 MHz, D_2O): δ = 6.31 (d, J = 1.6 Hz, 2H), 6.27 (t, J = 1.6 Hz, 1H), 3.87 (dd, J_1 = 4.0 Hz, J_2 = 6.4 Hz, 1H), 3.09 (dd, J_1 = 4.0 Hz, J_2 = 11.6 Hz, 1H), 2.90 (dd, J_1 = 6.4 Hz, J_2 = 11.6 Hz, 1H) ppm. ^{13}C NMR (126 MHz, D_2O): δ = 173.8, 157.2, 157.2, 138.1, 108.4, 108.4, 101.8, 55.7, 36.2 ppm. MS (ESI) *m/z:* calcd for $C_9H_{11}NO_4H^+$ = 197.19, found = 197.88 $[M+H]^+$, 219.90 $[M+Na]^+$, 235.08 $[M+K]^+$.

***Rac*-(7 b) 2,4-dihydroxyphenylalanine**,[29] $C_9H_{10}NO_4$ (196.18 g/mol). Hydrolysis is performed by reacting compound **6 b** in a 5 mL HBr solution (2 M). The reaction is refluxed overnight under an inert atmosphere. The solution is taken up in water and then the aqueous phase is washed with 3 x AcOEt and evaporated to dryness. The pure product is obtained after purification by HPLC as pinkish powder (10%).^{1}H NMR (500 MHz, D_2O): δ = 6.89 (d, J = 8 Hz, 1H), 6.29 (s, 1H), 6.27 (d, J = 2.3 Hz, 1H), 4.84 (dd, J_1 = 4.5 Hz, J_2 = 7.9 Hz, 1H), 3.09 (dd, J_1 = 4.5 Hz, J_2 = 14.7 Hz, 1H), 2.99 (dd, J_1 = 7.9 Hz, J_2 = 14.7 Hz, 1H) ppm. ^{13}C NMR (126 MHz, D_2O): δ = 172.6, 156.3, 155.5, 132.5, 113.2, 107.5, 102.7, 54.2, 30.3 ppm. MS (ESI) *m/z:* calcd for $C_9H_{10}NO_4H^+$ = 197.19, found = 198.01 [M + H], 196.00 $[M-H]^-$.

(8) (*S*)-*N*-(1-(2,4-dimethoxyphenyl)-3-oxo-3-((1-phenylethyl)-amino)-prop-1-en-2-yl)- benzamide, $C_{26}H_{26}N_2O_4$ (430.50 g/mol). To a solution of 7.67 g of **2 b** (24.80 mmol, 1 eq) in 75 mL of chloroform is added dropwise 9.02 g of (*S*)-(−)-phenylethylamine (74.40 mmol, 3 eq). The mixture is left under stirring at reflux for 5 h. The solution becomes clear and yellow. It is washed with a 0.1 M HCl solution, with brine and then dried with Na_2SO_4. A yellow oil is obtained. The pure product is purified by precipitation when adding ether and a few drops of dichloromethane to the crude mixture. The pure product is obtained in the form of a white powder with a yield of 70% (7.54 g).^{1}H NMR (400 MHz, chloroform-*d*): δ = 9.70 (s, NH), 8.33 (d, J = 8.3 Hz, NH), 7.99 (d, J = 7.5 Hz, 2H), 7.57 (t, J = 7.3 Hz, 1H), 7.54–7.46 (m, 3H), 7.42–7.36 (m, 3H), 7.32 (t, J = 7.5 Hz, 2H), 7.22 (t, J = 7.3 Hz, 1H), 6.59 (d, J = 2.5 Hz, 1H), 6.50–6.44 (m, 1H), 5.08 (p, J = 7.1 Hz, 1H), 3.83 (s, 3H), 3.75 (s, 3H), 1.42 (d, J = 7.1 Hz, 3H) ppm. ^{13}C NMR (100 MHz, chloroform-*d*): δ = 166.3, 165.1, 161.5, 159.0, 145.2, 134.4, 131.9, 130.00, 128.7, 128.5, 128.3, 126.8, 126.6, 124.1, 116.0, 105.6, 98.6, 56.1, 55.7, 48.6, 22.5 ppm. MS (ESI) *m/z:* calcd for $C_{26}H_{26}N_2O_4H^+$ = 431.50, found = 431.20 $[M+H]^+$, 453.19 $[M+Na]^+$, 469.18 $[M+K]^+$. M.p (°C): 71–74.

(9 b) *N*-((*S*)-3-(2,4-dimethoxyphenyl)-1-oxo-1-(((*S*)-1-phenylethyl)-amino)-propan-2-yl) benzamide, and **(9 b′) *N*-((*R*)-3-(2,4-dimethoxyphenyl)-1-oxo-1-(((*S*)-1-phenylethyl)-amino)-propan-2-yl) benzamide**, $C_{26}H_{28}N_2O_4$ (432.50 g/mol). A solution of 7.53 g of the compound **8** (17.51 mmol, 1eq) in 40 mL of methanol is hydrogenated at atmospheric pressure and room temperature over 0.75 g of Pd/C (10% by mass, 0.75 g). After 18 hours, the solvent is removed under reduced pressure and a white powder (5.36 g, 12.40 mmol) is obtained. The product is treated with boiling ethyl acetate and the remaining solid is hot filtered and consists in the pure diastereomer *(S,S)*-(**9 b**) is obtained in the form of a white solid with a cottony consistency (0.30 g, 4%). The second diastereomer *(S,R)*-(**9 b′**) crystallizes from the filtrate to give a white powder (1.03 g, 14%).

(S,S)-(**9 b**) ^{1}H NMR (400 MHz, chloroform-*d*) : δ = 8.30 (d, J = 11.4 Hz, NH), 8.30 (d, J_2 = 8.1 Hz, NH), 7.83–7.76 (m, 2H), 7.56–7.49 (m, 1H), 7.49–7.43 (m, 2H), 7.35–7.25 (m, 2H), 7.21 (d, J = 7.4 Hz, 3H), 7.07 (d, J = 8.3 Hz, 1H), 6.50 (d, J = 2.4 Hz, 1H), 6.37 (dd, J_1 = 8.3 Hz, J_2 = 2.4 Hz, 1H), 4.94 (p, J = 7.3 Hz, 1H), 4.69 (td, J_1 = 9.6 Hz, J_2 = 5.3 Hz, 1H), 3.77 (s, 3H), 3.71 (s, 3H), 3.00 (dd, J_1 = 13.8 Hz, J_2 = 5.3 Hz, 1H), 2.87 (dd, J_1 = 13.8 Hz, J_2 = 9.6 Hz, 1H), 1.37 (d, J = 7.3 Hz, 3H) ppm.^{13}C NMR (100 MHz, chloroform-*d*) : δ = 171.3, 167.5, 156.4, 158.3, 145.3, 133.6, 131.6, 131.7, 129.6, 128.7, 127.3, 126.9, 126.5, 114.7, 106.4, 55.7, 55.6, 55.3, 48.1, 48.0, 31.8, 22.8 ppm.

(S,R)-(**9 b′**) ^{1}H NMR (400 MHz, chloroform-*d*): δ = 8.32 (d, J = 8.1 Hz, NH), 8.23 (d, J = 8.1 Hz, NH), 7.81–7.76 (m, 2H), 7.56–7.49 (m, 1H), 7.45 (dd, J_1 = 8.2 Hz, J_2 = 6.8 Hz, 2H), 7.35–7.25 (m, 4H), 7.24–7.17 (m, 1H), 7.10 (d, J = 8.3 Hz, 1H), 6.52 (d, J = 2.4 Hz, 1H), 6.42 (dd, J_1 = 8.3 Hz, J_2 = 2.4 Hz, 1H), 4.89 (p, J = 7.2 Hz, 1H), 4.68 (td, J_1 = 8.8 Hz, J_1 = 5.6 Hz, 1H), 3.80 (s, 3H), 3.72 (s, 3H), 3.00 (dd, J_1 = 13.8 Hz, J_2 = 5.6 Hz, 1H, CH_2), 2.93 (dd, J_1 = 13.8 Hz, J_2 = 8.8 Hz, 1H, CH_2), 1.28 (d, J = 7.2 Hz, 3H) ppm. ^{13}C NMR (100 MHz, chloroform-*d*): δ = 170.2, 167.8, 160.1, 158.2, 143.0, 133.9, 131.9, 131.7, 128.5, 127.1, 127.0, 126.0, 117.7, 104.7, 98.8, 55.6, 55.4, 55.2, 50.9, 48.9, 31.6, 21.9 ppm. MS (ESI) *m/z:* calcd for $C_{26}H_{28}N_2O_4$ = 432.20, found = 433.24 $[M+H]^+$, 455.21 $[M+Na]^+$.

(10 b) *N*-((*S*)-3-(2,4-dihydroxyphenyl)-1-oxo-1-(((*S*)-1-phenylethyl)-amino)-propan-2-yl) benzamide, $C_{24}H_{24}N_2O_4$ (404.47 g/mol). The diastereomer *(S,S)*-(**9 b**) (1.03 g, 0.69 mmol) is placed in a flask in a nitrogen/acetone bath (− 95 °C) and under an inert atmosphere in 3 mL of anhydrous CH_2Cl_2. 0.9 mL of BBr_3 is added dropwise. The reaction is left to stir at room temperature overnight. Then, the excess of BBr_3 is destroyed at 0 °C with MeOH. After evaporation, the mixture is taken up in water and the product of interest is extracted with CH_2Cl_2. The final product is obtained in the form of a grey solid with a quantitative yield (0.95 g, 0.59 mmol).^{1}H NMR (500 MHz, DMSO-d_6) : δ = 9.44 (s, OH), 8.33–8.24 (m, 2H), 7.83–7.76 (m, 2H), 7.57–7.50 (m, 1H), 7.50–7.42 (m, 2H), 7.35–7.17 (m, 5H), 6.89 (dd, J_1 = 11.7 Hz, J_2 = 8.2 Hz, 1H), 6.29 (d, J = 2.4 Hz, 1H), 6.11 (ddd, J_1 = 11.7 Hz, J_2 = 8.2 Hz, J_3 = 2.4 Hz, 1H), 4.92 (dp, J_1 = 15.4 Hz, J_2 = 7.0 Hz, 1H), 4.60 (ddd, J_1 = 9.9 Hz, J_2 = 7.7 Hz, J_3 = 4.8 Hz, 1H), 2.92 (dd, J_1 = 13.9 Hz, J_2 = 4.8 Hz, 1H), 2.83 (dd, J_1 = 13.9 Hz, J_2 = 9.9 Hz, 1H), 1.37 (d, J = 7.0 Hz, 3H) ppm.^{13}C NMR (126 MHz, DMSO-d_6): δ = 171.1, 166.5, 157.33 156.4, 144.9, 134.6, 131.7, 131.62, 128.7, 128.7, 128.6, 128.6, 127.7, 127.7, 126.9, 126.4, 115.0, 106.5, 102.7, 55.1, 48.26 31.8, 22.8, 22.8 ppm.

(10 b′) *N*-((*R*)-3-(2,4-dihydroxyphenyl)-1-oxo-1-(((*S*)-1-phenylethyl)-amino)-propan-2-yl) benzamide, $C_{24}H_{24}N_2O_4$ (404.47 g/mol). The diastereomer *(R,S)*-(**9 b′**) (0.30 g, 0.69 mmol) is placed in a flask in a nitrogen/acetone bath (− 95 °C) and under an inert atmosphere in 3 mL of anhydrous CH_2Cl_2. 0.5 mL of BBr_3 is added dropwise. The reaction is left to stir at room temperature overnight. Then, the excess of BBr_3 is destroyed at 0 °C with MeOH. After evaporation, the mixture is taken up in water and the product of interest is extracted with CH_2Cl_2. The final product is obtained in the form of a grey solid with a quantitative yield (0.24 g, 0.59 mmol).^{1}H NMR (500 MHz, DMSO-d_6): δ = 9.48 (s, OH), 9.06 (s, OH), 8.29 (d, J = 7.7 Hz, NH), 8.21 (d, J = 8.1 Hz, NH), 7.80–7.75 (m, 2H), 7.53 (t, J = 7.5 Hz, 1H), 7.45 (t, J = 7.5 Hz, 2H), 7.34–7.26 (m, 5H), 6.90 (d, J = 8.2 Hz, 1H), 6.29 (d, J = 2.5 Hz, 1H), 6.12 (dd, J_1 = 8.2 Hz, J_2 = 2.5 Hz, 1H), 4.90 (t, J = 7.3 Hz, 1H), 4.59 (q, J = 8.2 Hz, 1H), 2.89 (d, J = 8.2 Hz, 2H), 1.31 (d, J = 7.3 Hz, 3H) ppm. ^{13}C NMR (126 MHz, DMSO-d_6): δ = 171.1,

166.5, 157.33 156.4, 144.9, 134.6, 131.7, 131.62, 128.7, 128.7, 128.6, 128.6, 127.7, 127.7, 126.9, 126.4, 115.0, 106.5, 102.7, 55.1, 48.26 31.8, 22.8, 22.8 ppm.

(7 b) (+)-(*S*)-2,4-dihydroxyphenylalanine. Hydrolysis of **10 b** (0.24 g, 0.59 mmol) is performed in a mixture of 24 mL of water and 2.4 mL of 48% HBr solution. The reaction is refluxed during 16 hours under an inert atmosphere. The solution is taken up in water and then the aqueous phase is washed with 3 × AcOEt and evaporated to dryness. The pure product is obtained after purification by HPLC as pinkish powder. ^{1}H NMR (400 MHz, D_2O) $\delta =$ 7.21–7.09 (m, 1H, Ar–H), 6.61–6.51 (m, 2H, Ar–H), 4.47 (dd, $J = 7.5$, 5.2 Hz, 1H, CHα), 3.38 (dd, $J = 14.7$, 5.3 Hz, 1H, CH_2), 3.17 (dd, $J =$ 14.7, 7.4 Hz, 1H, CH_2) ppm. ^{13}C NMR (126 MHz, D_2O) $\delta = 173.3$, 158.6, 157.7, 133.7, 114.1, 108.72, 104.9, 53.8, 31.05 ppm. $[\alpha]_D^{20} = +28.3$ ° (589 nm Na, water, 0.083 g/100 ml). HRMS (ESI): m/z $[M–H]^-$ calcd for $C_9H_{10}O_4N = 196.06153$, found = 196.06122.

(7 b′) (−)-(*R*)-2,4-dihydroxyphenylalanine. Hydrolysis of **10 b′** (0.95 g, 2.36 mmol) is performed in a mixture of 24 mL of water and 2.4 mL of 48% HBr solution. The reaction is refluxed during 30 hours under an inert atmosphere. The solution is taken up in water and then the aqueous phase is washed with 3 × AcOEt and evaporated to dryness. The pure product is obtained after purification by HPLC as pinkish powder. ^{1}H NMR (500 MHz, D_2O) $\delta =$ 7.03–6.98 (m, 1H, Ar–H), 6.38 (d, $J = 7.6$ Hz, 2H, Ar–H), 4.21 (dd, $J =$ 7.6, 5.1 Hz, 1H, CHα), 3.23 (dd, $J = 14.7$, 5.1 Hz, 1H, CH_2), 2.99 (dd, $J =$ 14.7, 7.6 Hz, 1H, CH_2) ppm. ^{13}C NMR (126 MHz, D_2O) $\delta = 172.2$, 156.4, 155.56, 132.6, 113.0, 107.6, 102.8, 53.9, 30.23 ppm. $[\alpha]_D^{20} = -26.9$ ° (589 nm Na, water, 0.07518 g/100 ml). HRMS (ESI): m/z $[M–H]^-$, calcd for $C_9H_{10}O_4N = 196.06153$, found = 196.06171.

Abbreviations

Ty	tyrosinase
TyH	human Tyrosinase
Tryp1	Tyrosinase-related protein 1
L-tyr	*L*-tyrosine
MM/GBSA	molecular mechanics/generalized born surface area

Author Contributions

The manuscript was written through contributions of all authors. All authors have given approval to the final version of the manuscript.

Acknowledgements

The authors gratefully acknowledge CDT-Cosmethic 2.0 an "Investissements d'Avenir" program (ANR-15-IDEX-02) for financial support and with a grant for C.F. and L.K. The authors are grateful to ICMG platform (UAR2607) for the analytical facilities (NMR, ESI-MS and X-Ray) and to CECIC for computing facilities. This work has been partially supported by the CBH-EUR-GS (ANR-17-EURE-003) program and the Labex Arcane (ANR-11-LABX-0003-01) in the framework of which this work was carried out. The authors acknowledge the use of the ESRF beamlines ID23-2, ID30 A-1, ID30 A-3 and ID30B through the in-house research programme, the platforms within the Partnership for Structural Biology (PSB) and the EMBL High-Throughput Crystallisation facility. Y–M.N. acknowledges an ESRF Ph.D. fellowship funded by InnovaXN, a EU Horizon 2020 MSCA COFUND programme (innovaxn.eu, grant agreement no. 847439). We thank Dr. Adrià Sánchez Morales for his careful proofreading.

Conflict of Interests

The authors declare no competing financial interest.

Keywords: human tyrosinase · tyrosinase inhibitor · organic synthesis · molecular modelling · X-ray crystallography

[1] W. T. Ismaya, H. J. Rozeboom, A. Weijn, J. J. Mes, F. Fusetti, H. J. Wichers, B. W. Dijkstra, *Biochemistry* **2011**, *50*, 5477–5486.
[2] N. Fujieda, S. Yabuta, T. Ikeda, T. Oyama, N. Muraki, G. Kurisu, S. Itoh, *J. Biol. Chem.* **2013**, *288*, 22128–22140.
[3] S. G. Mauracher, C. Molitor, R. Al-Oweini, U. Kortz, A. Rompel, *Acta Crystallogr. Sect. D* **2014**, *70*, 2301–2315.
[4] M. Sendovski, M. Kanteev, V. S. Ben-Yosef, N. Adir, A. Fishman, *J. Mol. Biol.* **2011**, *405*, 227–237.
[5] Y. Matoba, T. Kumagai, A. Yamamoto, H. Yoshitsu, M. Sugiyama, *J. Biol. Chem.* **2006**, *281*, 8981–8990.
[6] H. F. Son, S.-H. Lee, S. H. Lee, H. Kim, H. Hong, U.-J. Lee, P.-G. Lee, B.-G. Kim, K.-J. Kim, *ACS Catal.* **2018**, *8*, 10375–10382.
[7] Y. Li, Y. Wang, H. Jiang, J. Deng, *Proc. Nat. Acad. Sci.* **2009**, *106*, 17002–17006.
[8] A. Bijelic, M. Pretzler, C. Molitor, F. Zekiri, A. Rompel, *Angew. Chem. Int. Ed.* **2015**, *54*, 14677–14680.
[9] I. Kampatsikas, A. Bijelic, A. Rompel, *Sci. Rep.* **2019**, *9*, 4022.
[10] X. Lai, H. J. Wichers, M. Soler-Lopez, B. W. Dijkstra, *Angew. Chem. Int. Ed.* **2017**, *56*, 9812–9815.
[11] X. Lai, H. J. Wichers, M. Soler-Lopez, B. W. Dijkstra, *Chem. Eur. J.* **2018**, *24*, 47–55.
[12] E. I. Solomon, D. E. Heppner, E. M. Johnston, J. W. Ginsbach, J. Cirera, M. Qayyum, M. T. Kieber-Emmons, C. H. Kjaergaard, R. G. Hadt, L. Tian, *Chem. Rev.* **2014**, *114*, 3659–3853.
[13] A. Bijelic, A. Rompel, C. Belle, in *Ser. Chem. Energy Environ.*, World Scientific, **2019**, pp. 155–183.
[14] M. Rolff, J. Schottenheim, H. Decker, F. Tuczek, *Chem. Soc. Rev.* **2011**, *40*, 4077–4098.
[15] C. A. Ramsden, P. A. Riley, *Bioorg. Med. Chem.* **2014**, *22*, 2388–2395.
[16] C. Faure, A. du Moulinet d'Hardemare, H. Jamet, C. Belle, E. Bergantino, L. Bubacco, M. Benfatto, Simaan, J. A., Réglier, M., in *Copp. Bioinorg. Chem. Health Bioinspired Catal.*, World Scientific, **2023**.
[17] M. Yaar, *J. Invest. Dermatol.* **2013**, *133*, 11–13.
[18] V. N. Sehgal, G. Srivastava, *Int. J. Dermatol.* **2008**, *47*, 1041–1050.
[19] B. Roulier, B. Pérès, R. Haudecoeur, *J. Med. Chem.* **2020**, *63*, 13428–13443.
[20] T. Pillaiyar, V. Namasivayam, M. Manickam, S.-H. Jung, *J. Med. Chem.* **2018**, *61*, 7395–7418.
[21] E. Buitrago, R. Hardré, R. Haudecoeur, H. Jamet, C. Belle, A. Boumendjel, L. Bubacco, M. Réglier, *Curr. Top. Med. Chem.* **2016**, *16*, 3033–3047.
[22] S. Fogal, M. Carotti, L. Giaretta, F. Lanciai, L. Nogara, L. Bubacco, E. Bergantino, *Mol. Biotechnol.* **2015**, *57*, 45–57.
[23] R. Haudecoeur, A. Gouron, C. Dubois, H. Jamet, M. Lightbody, R. Hardré, A. Milet, E. Bergantino, L. Bubacco, C. Belle, M. Réglier, A. Boumendjel, *ChemBioChem* **2014**, *15*, 1325–1333.
[24] T. Mann, W. Gerwat, J. Batzer, K. Eggers, C. Scherner, H. Wenck, F. Stäb, V. J. Hearing, K.-H. Röhm, L. Kolbe, *J. Invest. Dermatol.* **2018**, *138*, 1601–1608.
[25] A. Garcia-Jimenez, J. A. Teruel-Puche, J. Berna, J. N. Rodriguez-Lopez, J. Tudela, P. A. Garcia-Ruiz, F. Garcia-Canovas, *Bioorg. Med. Chem.* **2016**, *24*, 4434–4443.
[26] S. Khatib, O. Nerya, R. Musa, M. Shmuel, S. Tamir, J. Vaya, *Bioorg. Med. Chem.* **2005**, *13*, 433–441.
[27] W. Ishioka, K. Nihei, *J. Mol. Struct.* **2022**, *1268*, 133668.

[28] J. P. Lambooy, *J. Am. Chem. Soc.* **1956**, *78*, 771–774.
[29] J. P. Lambooy, *J. Am. Chem. Soc.* **1954**, *76*, 133–138.
[30] D.-S. Kim, S.-Y. Kim, S.-H. Park, Y.-G. Choi, S.-B. Kwon, M.-K. Kim, J.-I. Na, S.-W. Youn, K.-C. Park, *Biol. Pharm. Bull.* **2005**, *28*, 2216–2219.
[31] S. Okombi, D. Rival, S. Bonnet, A.-M. Mariotte, E. Perrier, A. Boumendjel, *J. Med. Chem.* **2006**, *49*, 329–333.
[32] B. Roulier, I. Rush, L. M. Lazinski, B. Pérès, H. Olleik, G. Royal, A. Fishman, M. Maresca, R. Haudecoeur, *Eur. J. Med. Chem.* **2023**, *246*, 114972.
[33] O. Toussaint, K. Lerch, *Biochemistry* **1987**, *26*, 8567–8571.
[34] C. Washington, J. Maxwell, J. Stevenson, G. Malone, E. W. Lowe, Q. Zhang, G. Wang, N. R. McIntyre, *Arch. Biochem. Biophys.* **2015**, *577–578*, 24–34.
[35] J. L. Muñoz-Muñoz, F. Garcia-Molina, J. Berna, P. A. Garcia-Ruiz, R. Varon, J. Tudela, J. N. Rodriguez-Lopez, F. Garcia-Canovas, *Biochim. Biophys. Acta BBA-Proteins Proteomics* **2012**, *1824*, 647–655.
[36] E. Buitrago, C. Faure, M. Carotti, E. Bergantino, R. Hardré, M. Maresca, C. Philouze, N. Vanthuyne, A. Boumendjel, L. Bubacco, A. du Moulinet d'-Hardemare, H. Jamet, M. Réglier, C. Belle, *Eur. J. Med. Chem.* **2023**, *248*, 115090.
[37] J. Jumper, R. Evans, A. Pritzel, T. Green, M. Figurnov, O. Ronneberger, K. Tunyasuvunakool, R. Bates, A. Žídek, A. Potapenko, A. Bridgland, C. Meyer, S. A. A. Kohl, A. J. Ballard, A. Cowie, B. Romera-Paredes, S. Nikolov, R. Jain, J. Adler, T. Back, S. Petersen, D. Reiman, E. Clancy, M. Zielinski, M. Steinegger, M. Pacholska, T. Berghammer, S. Bodenstein, D. Silver, O. Vinyals, A. W. Senior, K. Kavukcuoglu, P. Kohli, D. Hassabis, *Nature* **2021**, *596*, 583–589.
[38] G. M. Morris, D. S. Goodsell, R. S. Halliday, R. Huey, W. E. Hart, R. K. Belew, A. J. Olson, *J. Comput. Chem.* **1998**, *19*, 1639–1662.
[39] C. Faure, H. Jamet, C. Belle, A. Moulinet d'Hardemare, *ChemistrySelect* **2020**, *5*, 14735–14740.
[40] X. Lai, M. Soler-Lopez, H. J. Wichers, B. W. Dijkstra, *PLoS One* **2016**, *11*, e0161697.
[41] E. Buitrago, C. Faure, L. Challali, E. Bergantino, A. Boumendjel, L. Bubacco, M. Carotti, R. Hardré, M. Maresca, C. Philouze, H. Jamet, M. Réglier, C. Belle, *Chem. Eur. J.* **2021**, *27*, 4384–4393.
[42] N. J. Kus, M. B. Dolinska, K. L. Young, E. K. Dimitriadis, P. T. Wingfield, Y. V. Sergeev, *PLoS One* **2018**, *13*, e0198247.
[43] T.-S. Chang, *Int. J. Mol. Sci.* **2009**, *10*, 2440–2475.
[44] M. Nanao, S. Basu, U. Zander, T. Giraud, J. Surr, M. Guijarro, M. Lentini, F. Felisaz, J. Sinoir, C. Morawe, A. Vivo, A. Beteva, M. Oscarsson, H. Caserotto, F. Dobias, D. Flot, D. Nurizzo, J. Gigmes, N. Foos, R. Siebrecht, T. Roth, P. Theveneau, O. Svensson, G. Papp, B. Lavault, F. Cipriani, R. Barrett, C. Clavel, G. Leonard, *J. Synchrotron Radiat.* **2022**, *29*, 581–590.
[45] D. Von Stetten, P. Carpentier, D. Flot, A. Beteva, H. Caserotto, F. Dobias, M. Guijarro, T. Giraud, M. Lentini, S. McSweeney, A. Royant, S. Petitdemange, J. Sinoir, J. Surr, O. Svensson, P. Theveneau, G. A. Leonard, C. Mueller-Dieckmann, *J. Synchrotron Radiat.* **2020**, *27*, 844–851.
[46] A. A. McCarthy, R. Barrett, A. Beteva, H. Caserotto, F. Dobias, F. Felisaz, T. Giraud, M. Guijarro, R. Janocha, A. Khadrouche, M. Lentini, G. A. Leonard, M. Lopez Marrero, S. Malbet-Monaco, S. McSweeney, D. Nurizzo, G. Papp, C. Rossi, J. Sinoir, C. Sorez, J. Surr, O. Svensson, U. Zander, F. Cipriani, P. Theveneau, C. Mueller-Dieckmann, *J. Synchrotron Radiat.* **2018**, *25*, 1249–1260.
[47] M. W. Bowler, D. Nurizzo, R. Barrett, A. Beteva, M. Bodin, H. Caserotto, S. Delagenière, F. Dobias, D. Flot, T. Giraud, N. Guichard, M. Guijarro, M. Lentini, G. A. Leonard, S. McSweeney, M. Oskarsson, W. Schmidt, A. Snigirev, D. Von Stetten, J. Surr, O. Svensson, P. Theveneau, C. Mueller-Dieckmann, *J. Synchrotron Radiat.* **2015**, *22*, 1540–1547.
[48] P. A. Kollman, I. Massova, C. Reyes, B. Kuhn, S. Huo, L. Chong, M. Lee, T. Lee, Y. Duan, W. Wang, O. Donini, P. Cieplak, J. Srinivasan, D. A. Case, T. E. Cheatham, *Acc. Chem. Res.* **2000**, *33*, 889–897.
[49] S. Genheden, U. Ryde, *Expert Opin. Drug Discovery* **2015**, *10*, 449–461.
[50] J. L. Muñoz-Muñoz, F. Garcia-Molina, P. A. Garcia-Ruiz, R. Varon, J. Tudela, J. N. Rodriguez-Lopez, F. Garcia-Canovas, *Biochim. Biophys. Acta BBA-Proteins Proteomics* **2011**, *1814*, 1974–1983.
[51] B. Gasowska, P. Kafarski, H. Wojtasek, *Biochim. Biophys. Acta BBA - Gen. Subj.* **2004**, *1673*, 170–177.
[52] G. M. Morris, R. Huey, W. Lindstrom, M. F. Sanner, R. K. Belew, D. S. Goodsell, A. J. Olson, *J. Comput. Chem.* **2009**, *30*, 2785–2791.
[53] Frisch, M. J.; Trucks, G. W.; Schlegel, H. B.; Scuseria, G. E.; Robb, M. A.; Cheeseman, J. R.; Scalmani, G.; Barone, V.; Petersson, G. A.; Nakatsuji, H.; Li, X.; Caricato, M.; Marenich, A. V.; Bloino, J.; Janesko, B. G.; Gomperts, R.; Mennucci, B.; Hratchian, H. P.; Ortiz, J. V.; Izmaylov, A. F.; Sonnenberg, J. L.; Williams-Young, D.; Ding, F.; Lipparini, F.; Egidi, F.; Goings, J.; Peng, B.; Petrone, A.; Henderson, T.; Ranasinghe, D.; Zakrzewski, V. G.; Gao, J.; Rega, N.; Zheng, G.; Liang, W.; Hada, M.; Ehara, M.; Toyota, K.; Fukuda, R.; Hasegawa, J.; Ishida, M.; Nakajima, T.; Honda, Y.; Kitao, O.; Nakai, H.; Vreven, T.; Throssell, K.; Montgomery, J. A., Jr.; Peralta, J. E.; Ogliaro, F.; Bearpark, M. J.; Heyd, J. J.; Brothers, E. N.; Kudin, K. N.; Staroverov, V. N.; Keith, T. A.; Kobayashi, R.; Normand, J.; Raghavachari, K.; Rendell, A. P.; Burant, J. C.; Iyengar, S. S.; Tomasi, J.; Cossi, M.; Millam, J. M.; Klene, M.; Adamo, C.; Cammi, R.; Ochterski, J. W.; Martin, R. L.; Morokuma, K.; Farkas, O.; Foresman, J. B.; Fox, D. J., **2016**.
[54] T.-S. Lee, D. S. Cerutti, D. Mermelstein, C. Lin, S. LeGrand, T. J. Giese, A. Roitberg, D. A. Case, R. C. Walker, D. M. York, *J. Chem. Inf. Model.* **2018**, *58*, 2043–2050.
[55] W. L. Jorgensen, J. Chandrasekhar, J. D. Madura, R. W. Impey, M. L. Klein, *J. Chem. Phys.* **1983**, *79*, 926–935.
[56] J. A. Maier, C. Martinez, K. Kasavajhala, L. Wickstrom, K. E. Hauser, C. Simmerling, *J. Chem. Theory Comput.* **2015**, *11*, 3696–3713.
[57] C. Bochot, E. Favre, C. Dubois, B. Baptiste, L. Bubacco, P.-A. Carrupt, G. Gellon, R. Hardré, D. Luneau, Y. Moreau, A. Nurisso, M. Réglier, G. Serratrice, C. Belle, H. Jamet, *Chem. Eur. J.* **2013**, *19*, 3655–3664.
[58] D. R. Roe, T. E. Cheatham, *J. Chem. Theory Comput.* **2013**, *9*, 3084–3095.
[59] A. Onufriev, D. Bashford, D. A. Case, *Proteins Struct. Funct. Bioinf.* **2004**, *55*, 383–394.
[60] J. Gabadinho, A. Beteva, M. Guijarro, V. Rey-Bakaikoa, D. Spruce, M. W. Bowler, S. Brockhauser, D. Flot, E. J. Gordon, D. R. Hall, B. Lavault, A. A. McCarthy, J. McCarthy, E. Mitchell, S. Monaco, C. Mueller-Dieckmann, D. Nurizzo, R. B. G. Ravelli, X. Thibault, M. A. Walsh, G. A. Leonard, S. M. McSweeney, *J. Synchrotron Radiat.* **2010**, *17*, 700–707.
[61] J. Agirre, M. Atanasova, H. Bagdonas, C. B. Ballard, A. Baslé, J. Beilsten-Edmands, R. J. Borges, D. G. Brown, J. J. Burgos-Mármol, J. M. Berrisford, P. S. Bond, I. Caballero, L. Catapano, G. Chojnowski, A. G. Cook, K. D. Cowtan, T. I. Croll, J. É. Debreczeni, N. E. Devenish, E. J. Dodson, T. R. Drevon, P. Emsley, G. Evans, P. R. Evans, M. Fando, J. Foadi, L. Fuentes-Montero, E. F. Garman, M. Gerstel, R. J. Gildea, K. Hatti, M. L. Hekkelman, P. Heuser, S. W. Hoh, M. A. Hough, H. T. Jenkins, E. Jiménez, R. P. Joosten, R. M. Keegan, N. Keep, E. B. Krissinel, P. Kolenko, O. Kovalevskiy, V. S. Lamzin, D. M. Lawson, A. A. Lebedev, A. G. W. Leslie, B. Lohkamp, F. Long, M. Malý, A. J. McCoy, S. J. McNicholas, A. Medina, C. Millán, J. W. Murray, G. N. Murshudov, R. A. Nicholls, M. E. M. Noble, R. Oeffner, N. S. Pannu, J. M. Parkhurst, N. Pearce, J. Pereira, A. Perrakis, H. R. Powell, R. J. Read, D. J. Rigden, W. Rochira, M. Sammito, F. Sánchez Rodríguez, G. M. Sheldrick, K. L. Shelley, F. Simkovic, A. J. Simpkin, P. Skubak, E. Sobolev, R. A. Steiner, K. Stevenson, I. Tews, J. M. H. Thomas, A. Thorn, J. T. Valls, V. Uski, I. Usón, A. Vagin, S. Velankar, M. Vollmar, H. Walden, D. Waterman, K. S. Wilson, M. D. Winn, G. Winter, M. Wojdyr, K. Yamashita, *Acta Crystallogr. Sect. Struct. Biol.* **2023**, *79*, 449–461.
[62] D. Liebschner, P. V. Afonine, M. L. Baker, G. Bunkóczi, V. B. Chen, T. I. Croll, B. Hintze, L.-W. Hung, S. Jain, A. J. McCoy, N. W. Moriarty, R. D. Oeffner, B. K. Poon, M. G. Prisant, R. J. Read, J. S. Richardson, D. C. Richardson, M. D. Sammito, O. V. Sobolev, D. H. Stockwell, T. C. Terwilliger, A. G. Urzhumtsev, L. L. Videau, C. J. Williams, P. D. Adams, *Acta Crystallogr. Sect. Struct. Biol.* **2019**, *75*, 861–877.
[63] P. Emsley, *Acta Crystallogr. Sect. Struct. Biol.* **2017**, *73*, 203–210.
[64] E. Marková, M. Kotik, A. Křenková, P. Man, R. Haudecoeur, A. Boumendjel, R. Hardré, Y. Mekmouche, E. Courvoisier-Dezord, M. Réglier, L. Martínková, *J. Agric. Food Chem.* **2016**, *64*, 2925–2931.

Manuscript received: March 13, 2024
Revised manuscript received: April 18, 2024
Accepted manuscript online: April 20, 2024
Version of record online: June 7, 2024